1.0

1.1

1.25

4.5
5.0
5.6
6.3

2.8
3.2
3.6
4.0

2.5
2.2
2.0
1.8

1.4

1.6

MICROCOPY RESOLUTION TEST CHART
NATIONAL BUREAU OF STAND

CHARACTERIZATION OF LASER ANNEALING
OF ION IMPLANTED GaAs AND Si
USING OPTICAL REFLECTIVITY

THESIS

AFIT/GEP/PH/79D-6   Bill W. Mullins
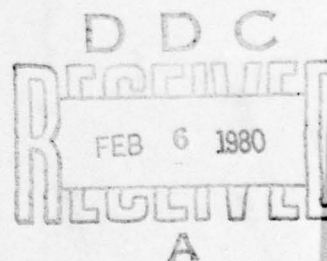   2Lt   USAF

D D C
RECEIVED
FEB 6 1980

A

Approved for public release; distribution umlimited.

CHARACTERIZATION OF LASER ANNEALING

OF ION IMPLANTED GaAs AND Si

USING OPTICAL REFLECTIVITY.

Master's THESIS,

Presented to the Faculty of the School of Engineering

of the Air Force Institute of Technology

Air University (ATC)

in Partial Fulfillment of the

Requirements for the Degree of

Master of Science

by

Bill W. Mullins, B.S.

2nd Lt   USAF

Graduate Engineering Physics

December 1979

Approved for public release; distribution unlimited.

Preface

On a national scale, the results of this thesis represent a small step forward in the understanding of laser annealing of ion implanted semiconductors. However, the results do indicate that reflectivity may be better than previous techniques for characterizing the damage profiles in the implanted substrate. These results would not be possible without the help of many dedicated professional people.

My thanks go to Messrs. Jim Miskimen, George Gergal, and Ron Gabriel for their expertise in setting up and operating the necessary equipment. I would also like to thank Mr. David Walsh for his help in producing a satisfactory reference mirror. My very special thanks go to Dr. Robert Hengehold, my faculty advisor, whose expert guidance was always available when it was needed.

My highest praise goes to my wife, Jill. Her constant reassurance during the dark times that occur in any research project was a great factor in keeping my morale and hopes high. For her continued support and help throughout every phase of this thesis I will be greatly indebted.

Contents

List of Figures

Abstract

The effect of laser annealing on ion implanted GaAs and Si has been assessed using optical reflectivity spectra. The spectra were recorded over the range of 2100Å to 4500Å and reflectivity peaks were obtained near 2400Å and 4100Å for GaAs and 2700Å and 3700Å for Si. The magnitude of these peaks was then observed as a function of annealing parameters. Laser annealing was carried out using a 30 nsec ruby laser pulse. The GaAs samples were implanted with 120 KeV Te at a fluence of 10^{14} ions/cm^2; Si samples were implanted with 30 KeV In at a fluence of 10^{15} ions/cm^2. The reflectivity spectrum of implanted GaAs was found to return to that of the unimplanted materials at an annealing energy density of approximately 0.35 J/cm^2 whereas the spectrum of Si was found to approach that of the unimplanted sample at energy densities of 1.34 J/cm^2. The values obtained compare well with those obtained from other diagnostic techniques.

I Introduction

A key part in today's Air Force planning is the versitility, reliability, and size of electronic equipment. Semiconductor technology has greatly improved the versitility and reliability, and decreased the size of electronic components. However, to meet the needs of the future, the Air Force will need even more sophisticated, more reliable, and smaller electronic packages. To meet the needs of the present and future, better p and n type layers and p-n junctions are required.

The formation of the above junctions depends upon the purity, concentration, and distribution of dopants added to a substrate. Two commonly used substrate materials are Silicon (Si) and Gallium Arsenide (GaAs). There are several methods of doping the substrate materials, such as: (1) crystal growth from a doped mixture, (2) thermal diffusion of the dopant into the substrate, (3) producing a dopant-substrate alloy in the substrate, and (4) ion implantation.

Ion implantation is an especially attractive doping scheme since it is the only process that introduces a pure dopant into the substrate. The implantation process also allows control over the dopant profile in the substrate and a more precise control of the dopant dose. However, the implantation process does have drawbacks. Upon implanting the surface of the crystal, the long range order in the doped layers of the crystal is destroyed, and it is this order that produces the desired electrical properties of the semiconductor. Thus the implantation damage must be repaired.

The repairing of the damaged layers in an implanted crystal is called annealing. Presently, two types, thermal and laser annealing, are

1

proposed. Thermal annealing of ion implanted layers, while successful, has its drawbacks. It is time consuming and can change the dopant profile. On the other hand, laser annealing is very fast and could possibly do a better job of annealing the surface of the crystal than the thermal process.

The purpose of this thesis is to study the regrowth, or repairing, of the ion implanted regions in Si and GaAs using optical reflectivity measurements. Contained in the following sections are discussions on implanting and annealing crystals, why optical reflectivity should be a good tool to study the regrowing process, experimental set up and procedure, results and conclusions, and finally, recommendations. Several graphs of the reflectivity, $R(\omega)$, as a function of the frequency of the incident light, ω, are presented for several different conditions for the crystal. Also, a comparison of the changes in $R(\omega)$ as a function of laser annealing energy density is compared to changes in other parameters of the crystal such as the extinction coefficient and electrical activation.

2

II Theory

Ion Implantation

Of the several doping methods for semiconductors, ion implantation seems to be the best. Only this method allows a pure dopant to be introduced into the substrate and precise control of the dopant profile.

The implantation process requires that ions of sufficient momentum collide with, and stick in, the lattice of the crystal. For the dopant ions to stick in the lattice, they must undergo inelastic collisions with the atoms of the crystal, transferring their kinetic energy to the crystal lattice. The inelastic collisions occur when the lattice bonds are broken, displacing an atom from its regular lattice position, or when collisions between the substrate atoms and the dopant ions causes the substrate atoms to oscillate, heating up the crystal. Thus, by undergoing several collisions, the dopant ion loses all of its kinetic energy and stays in the substrate. However, for the dopant to reach any depth in the crystal, a fairly high momentum ion must be used.

High momentum ions can be produced with a medium energy ion accelerator. In the accelerator, a plasma of the chosen dopant is formed and the ions are accelerated to kinetic energies of 10 to 100's of KeVs. This beam is then separated into its component parts using a charge to mass ratio selector. Since the charge to mass ratio of an element is unique, then only those nuclei with the proper e/m ratio will be passed through the selector. This selector could be as simple as a magnetic field lying perpendicular to the velocity of the ion beam. By adjusting the magnetic field, the angle of deflection for any e/m ratio can be varied and the needed dopant ions brought to bear on the substrate material.

3

This, and other types of selectors will exclude all other types of ions from striking the crystal due to the uniqueness of the e/m ratio for each nuclei.

By controlling the energy of the ion beam, hence the momentum, the depth of average penetration into the substrate is controlled. The concentration, as a function of depth in the substrate, will assume the form of a gaussian. The position of the peak concentration can be controlled by adjusting the momentum of the incident ion (Ref 1). Also, the total number of ions, d, can be controlled by knowing the current density of the ion beam, J, and exposure time, t, of the crystal to the beam such that:

$$d(ions/cm^3) = qJ(ions/cm^3-sec)t(sec) \tag{1}$$

Where q is the sticking efficiency, or percentage of incident ions that remain in the substrate. Thus, the dopant purity, dose, and density profile in the substrate can be controlled.

However, the implantation process damages the surface layers of the crystal. Implanted ions rarely go into a substitutional site, therefore greatly increasing the number of scattering centers in the lattice. This increase in scattering centers does, at sufficiently large doses, destroy all long, and even short, range order in the crystal, producing an amorphous like layer in the implanted region (Ref 2). Destruction of this long range order seriously affects the normal properties of the crystalline substrate, hence, this order must be restored.

Annealing

To restore the normal crystalline properties, the long range order must be reestablished in the doped layers. This process is called

4

annealing. Annealing is done by heating the damaged area such that the atoms have sufficient energy to move, allowing the dopant atoms to occupy substitutional sites, while allowing the substrate atoms to stay in normal lattice positions.

Thermal annealing is a process in which the entire crystal is heated in a high temperature oven. Implanted Si is reported to have little damage after thermal annealing (Ref 3). However, temperatures of upwards to 1000°C for one hour are sometimes needed for complete thermal annealing. At these temperatures an inert atmosphere is needed to avoid gross contamination of the crystal. Also, the annealing periods allow ample time for the dopant to diffuse into, or out of, the crystal, changing the dopant profile.

Laser annealing is another means of repairing the implantation damage. The damaged layers could be adequately heated by a sufficiently energetic laser beam. The very fast surface heating with the laser implies that the entire crystal does not have to be heated, thus preventing diffusion of the dopant deeper into the crystal. With only the surface heated by the laser, the rest of the crystal can act as a heat sink, therefore rapidly cooling the surface and not allowing the dopant time to significantly diffuse out of the crystal (Ref 4). With these shorter melt times, 10 - 100 nsec, there should be little time for oxidation. Thus eliminating the need for an inert annealing atmosphere.

There are, however, conflicting reports on the success of laser annealing. Reported Rutherford backscattering (RBS) measurements show a significant regrowth in the amorphous layer in ion implanted, laser annealed Si with 60% of the dopant occupying regular lattice positions (Ref 4). Yet, weak spectral lines from cathodoluminescence of GaAs imply that the

5

number of nonradiative centers is high, indicating that the regrowth in laser annealed, ion implanted GaAs layers is not complete (Ref 5). Although RBS indicates the order has been restored in the lattice, it is not sensitive to defects such as vacancies, clusters, etc., like cathodoluminescence. Yet, for cathodoluminescence to be efficient, a high degree of crystalline perfection is required. Therefore, an experimental technique that is more sensitive to crystalline defects than RBS, but not as sensitive as cathodoluminescence, is implied for studying the regrowth of the implanted layers.

Recent studies of the change in the extinction coefficient of the complex index of refraction of ion implanted, laser annealed GaAs has shown a correlation between the regrowth in the damaged layers and the onset of electrical activation (Ref 6). Since the reflectivity spectrum of a crystal is dependent upon the extinction coefficient, changes in this coefficient should produce changes in the reflectance spectrum, as we shall show later. Therefore, reflectivity should be a useful tool in studying the regrowth of the damaged layers.

Reflectivity

The reflectivity, R, of a substance is defined as the ratio of the reflected, I_r, to the incident, I_o, intensities from a surface such that:

$$R \equiv I_r/I_o \tag{2}$$

Fresnel showed that the reflectivity for non-conducting media has the form

$$R_\perp = |r_\perp|^2 = \left| \frac{n_2\cos\theta_i - n_1\cos\theta_t}{n_2\cos\theta_i + n_1\cos\theta_t} \right|^2 \tag{3}$$

6

$$R_{\shortparallel} = |r_{\shortparallel}|^2 = \left| \frac{n_1 \cos\theta_i - n_2 \cos\theta_t}{n_1 \cos\theta_i + n_2 \cos\theta_t} \right|^2 \tag{4}$$

where θ_i and θ_t are the angles of incidence and refraction; n_2 and n_1 are the index of refraction for the absorbing and surrounding mediums; and $\shortparallel$ and $\perp$ refer to the components parallel and perpendicular to the plane of incidence, respectively. These equations are derived by applying the appropriate boundary conditions to electromagnetic fields at the common interface of the two media, separately for each direction of polarization. Since these equations are derived using the linear relationships between field vectors, then for a conducting media the equations have the same form. Thus the index of refraction for a conductor must be known.

The general equation for propagation of electromagnetic waves through a medium of finite conductivity is

$$\nabla^2 E - \sigma\mu \frac{\partial E}{\partial t} - \mu\epsilon \frac{\partial^2 E}{\partial_t^2} = 0 \tag{5}$$

where E is the electric field, σ is the conductivity, μ is the permeability, and ϵ is the permittivity of the medium (Ref 7). A similar equation can be written for H. Assuming a monochromatic plane wave of angular frequency, ω, the solution takes the form

$$E = E_o \exp[i\omega(t - x/v)] \tag{6}$$

where v is the velocity of the wave in the medium, putting Eq (6) into Eq (5), we find that

$$1/v^2 = \mu(\epsilon - i\sigma/\omega) \tag{7}$$

7

If we want the relationship $v = c/n$ to hold, then n must be complex, thus we define

$$\hat{n} = n+ik \qquad (8a)$$

where n is the index of refraction, k is the extinction coefficient and both are real. Other relationships can also be taken as definitions, i.e.

$$c^2 = \frac{1}{\mu_o \varepsilon_o}, \quad K_m = \frac{\mu}{\mu_o}, \quad K_e = \frac{\varepsilon}{\varepsilon_o} \qquad (8b)$$

where c is the speed of light, μ_o and ε_o are the free space values, K_m is the relative permeability, and K_e is the relative permittivity. Using these relationships along with Eqs (7) and (8a) we get

$$\hat{n}^2 = n^2 - i2nk - k^2 = K_m(K_e - i\sigma/\varepsilon_o \omega) \qquad (9)$$

For non-magnetic material $K_m = 1$, and Eq (9) becomes

$$\hat{n}^2 = K_e - i\sigma/\varepsilon \omega \qquad (10)$$

Equating real and imaginary parts we find that

$$n^2 - k^2 = K_e \qquad (11)$$

and

$$2nk = \sigma/\varepsilon_o \omega \qquad (12)$$

By using Eq (12), we can write n in terms of k and get a quadratic in n^2. A similar equation can be written for k^2 and we can solve for n and k where:

$$2n^2 = K_e \left[1 + \sqrt{1 + \left(\frac{\sigma}{\varepsilon_o \omega K_e} \right)^2} \right] \tag{13}$$

and

$$2K^2 = K_e \left[-1 + \sqrt{1 + \left(\frac{\sigma}{\varepsilon_o \omega K_e} \right)^2} \right] \tag{14}$$

Thus we know the complex index of refraction for a conducting media, and Eqs (3) and (4) become

$$R_\perp = \left| \frac{(n+ik)\cos\theta_i - n_1 \cos\theta_t}{(n+ik)\cos\theta_i + n_1 \cos\theta_t} \right|^2 \tag{15}$$

and

$$R_{\parallel} = \left| \frac{n_1 \cos\theta_i - (n+ik)\cos\theta_t}{n_1 \cos\theta_i + (n+ik)\cos\theta_t} \right|^2 \tag{16}$$

and θ_i is related to θ_t by Snell's law.

From Eqs (10), (13), and (14), it is clear that in a conducting medium, $\hat{n}$ is a function of ω, implying that R is also a function of ω. To understand $\hat{n} = \hat{n}(\omega)$, we must look inside the crystal, to find the relationship between the fundamental electrical properties of and the optical dispersion in a conducting media.

Dispersion in a semiconductor arises from bound and free electrons. The free electrons contribute primarily to the long wavelength absorption bands and the bound electrons contribute to the absorption at energies higher than the fundamental absorption edge, the region of interest in this experiment.

9

The motion of the bound electron can be described by the classical Lorentz oscillator. Consider a collection of similar charges bound in a linear, isotropic, and homogeneous crystal lattice. Thus, there are no preferred directions of motion for the electrons. Therefore, the electronic motion will always be in the direction of the applied field and hence we only need to work with the amplitude of the displacement. Given a local field of the form

$$E = E_o \exp[-i\omega t] \tag{17}$$

the motion of the system can be described by the equation

$$m\frac{\partial^2 r}{\partial t^2} + m\gamma\frac{\partial r}{\partial t} + m\omega_o^2 r = -eE \tag{18}$$

where m, ω_o, and e are the electron's mass, resonant frequency, and charge magnitude, respectively. The term $m\gamma(dr/dt)$ is an energy loss mechanism. Two approximations have been made in Eq (18). Since the electron works against the entire crystal lattice, the mass of the nucleus is assumed infinite. The small force $e\vec{v} \times \vec{B}/c$ is neglected, since the velocity of the electron is small compared to c (Ref 8). Assuming a periodic displacement, the solution to Eq (18) becomes:

$$r = \frac{eE}{m}(\omega_o^2 - \omega^2 - i\gamma\omega)^{-1} \tag{19}$$

Thus the magnitude of induced dipole moment, p, is

$$p = \frac{e^2 E}{m}(\omega_o^2 - \omega^2 - i\gamma\omega)^{-1} \tag{20}$$

10

If the electrons are considered to be associated with the molecules of a dielectric, such that there are N oscillators per unit volume, the dielectric may be modeled as a collection of dipoles with an average dipole moment per unit volume, P:

$$P = N<p> \tag{21}$$

To relate the microscopic atomic polarizability to the macroscopic polarization, the relationship between the microscopic local E field and the macroscopic incident E field must be known. Except for ideal cases, this is a considerably complex problem. For our treatment, we will assume a small displacement in r which will allow us to equate the incident field to the time average of the local field (Ref 8). Thus, from Eqs (20) and (21), it is seen that the polarizability is complex, with an energy loss mechanism. This implies that $\vec{E}$, $\vec{D}$, and $\vec{P}$ are no longer in phase. Thus, $\vec{D}$ must be generalized to a complex form:

$$\vec{D} = \epsilon\vec{E} = \vec{E} + 4\pi\vec{P} \tag{22}$$

Now from Eqs (20), (21), and (22) we have that

$$\hat{\epsilon} = 1 + \frac{4\pi N e^2}{m}(\omega_o^2 - \omega^2 - i\gamma\omega)^{-1} \tag{23}$$

where $\hat{\epsilon}$ is the complex dielectric function.
Also, $\hat{\epsilon}$ can be written as

$$\hat{\epsilon} = \epsilon_1 + i\epsilon_2 = \epsilon_o\hat{n}^2 = \epsilon_o(n + ik)^2 \tag{24}$$

in an isotropic media (Ref 9). Thus equating real and imaginary parts in Eqs (23) and (24) we have

11

$$\epsilon_1 = n^2 - k^2 = 1 + \frac{4\pi N e^2}{m} \frac{(\omega_o^2 - \omega^2)}{(\omega_o^2 - \omega^2)^2 + \gamma^2 \omega^2} \tag{25}$$

$$\epsilon_2 = 2nk = \frac{4\pi N e^2}{m} \frac{\gamma \omega}{(\omega_o^2 - \omega^2)^2 + \gamma^2 \omega^2} \tag{26}$$

Now consider the crystal to contain j different oscillators, f_j in number, with characteristic constants, ω_j and γ_j. Then the total effect is the sum of the individual contributors, and Eq (23) becomes

$$\hat{\epsilon} = 1 + \frac{4\pi e^2}{m} \sum_j \frac{f_j N_j}{(\omega_j^2 - \omega^2) - i \gamma_j \omega} \tag{27}$$

$$\sum_j N_j = N \tag{28}$$

Eq (27) is the fundamental result of classical dispersion theory. If one applies a rigorous quantum mechanical analysis to the system, an identical equation results, with different physical interpretations to the constants. In the quantum mechanical approach, ω_j is the transition frequency between two states separated by $\hbar \omega_j$ in energy, and f_j is the oscillator strength, or transition probability, for the electron. Now, for a single oscillator, consider the frequency dependence of ϵ_1 and ϵ_2, n and k, and R, at normal incidence, shown in Figures 1, 2, and 3, respectively, for $\hbar \omega = 4eV$, $\hbar \gamma = 1eV$, and $4\pi N e^2/m = 60$ (Ref 8). Notice in Figures 2 and 3 that as k increases, so does the absorption and reflectivity. Thus, as the electrons start to absorb the incident radiation, they are excited, start a harmonic resonance, and reemit the incident radiation. Therefore, the reflectance reaches a peak value near the resonant frequency ω_j. If f_j is not the same

12

for all oscillators, then some frequencies will have stronger absorption and reflectance than others, hence a reflectance spectrum (Fig 4).

Since the periodic internal field of the crystal is responsible for the band structure and reflectivity spectrum, optical reflectivity should be a good tool to measure the regrowth of the amorphous layers. As the implantation ruins the long range order, there are smaller areas in the crystal with enough order to retain $R(\omega)$ of the original crystal. As the dopant dose increases, the reflectance of the amorphous surface starts to superimpose itself on top of $R(\omega)$ for the crystal. At high doses there is no longer enough order in the crystal for $R(\omega)$ to be detected. As the crystal is annealed, then $R(\omega)$ starts to reappear as order is reestablished in the implanted layers. As annealing continues, $R(\omega)$ will be more pronounced until the crystal is fully annealed and $R(\omega)$ for the implanted lattice looks identical to that of a virgin, or unimplanted, sample.

Problems do arise in $R(\omega)$ measurements due to thin film interactions on the crystal surface. Avoidance of these films is not a trivial task, since exposure to the atmosphere can form oxide layers. Thus, some measurement of the $R(\omega)$ curve must be found that looks strictly at the crystallinity, not surface effects. One possible parameter is relative peak height. Comparing the peak to valley difference in R could give a measure of the crystallinity. As this difference increases, so does the order in the crystal.

Miyao, et al (Ref 2), describes a damage criteria, D, such that $D = 0$ for a crystalline sample, and $D = 1$ for an amorphous sample. The damage to the surface of the crystal is given by

13

$$D = \frac{(R_1^c - R_2^c)/R_2^c - (R_1^s - R_2^s)/R_2^s}{(R_1^c - R_2^c)/R_2^c - (R_1^a - R_2^a)/R_2^a} \tag{29}$$

where R_1 and R_2 denote the reflectance at the peak and valley of a crystal, respectively. Superscripts c and a represent the standard samples for crystalline and amorphous layers, and s represents the sample under investigation. For Si, R_1 and R_2 are at 275.5 nm and 330.0 nm, respectively, and for GaAs, R_1 and R_2 are at 246.5 nm and 310.0 nm, respectively. Thus, D should represent a damage parameter which is sensitive to the crystallinity of the sample, and yet relatively insensitive to surface films. However, the value of D is good only for the depth that the incident beam attains in the crystal.

The intensity of a wave travelling through a conducting media is described by the equation

$$I = I_o \exp\left[\frac{-4\pi k}{\lambda} x\right] \tag{30}$$

where x is the distance in the medium and λ is the wavelength of the travelling wave (Ref 10). For GaAs, the depth of penetration of I_o is 6 nm at $\lambda = 248$ nm. Hence, the crystallinity, measured by Eq (29), of the sample is for only the first few layers of the crystal. By redefining R_1 in Eq (29) to correspond to a peak in $R(\omega)$ at a longer wavelength, the crystallinity of the sample could be measured at a deeper distance.

Hence, this damage parameter will be used to look at the regrowth of the amorphous layer with increasing energy density, E_d, of the annealing laser beam. Therefore, as E_d increases, then D should decrease until a full anneal is achieved. If it is possible to get E_d high enough, then

14

damage to the crystal surface from the laser should be possible, thus bracketing the optimum value for E_d for complete, or best, one shot annealing.

Previous reflectivity studies of ion implanted Si show that with increasing dose, the structure in $R(\omega)$ disappears (Ref 3). Also, D increases with increasing dose up to fluences of 5×10^{14} ions/cm^2 where D = 1 and the implanted region is completely amorphous (Ref 2). Upon thermal annealing, $R(\omega)$, for implanted Si, regains most of its structure and, under proper annealing conditions, is identical to $R(\omega)$ for a virgin sample (Ref 3). Kim, et al (Ref 6), has found that the extinction coefficient, k, for laser annealed, ion implanted GaAs comes to within 0.2 of the value of k for thermally annealed implanted GaAs at annealing energy densities of 0.2 J/cm^2. Electrical activation was also found to start at annealing energy densities of 0.3 J/cm^2 for implanted GaAs (Ref 6). Hence, changes have been observed in the reflectance spectra of thermal and laser annealed ion implanted samples.
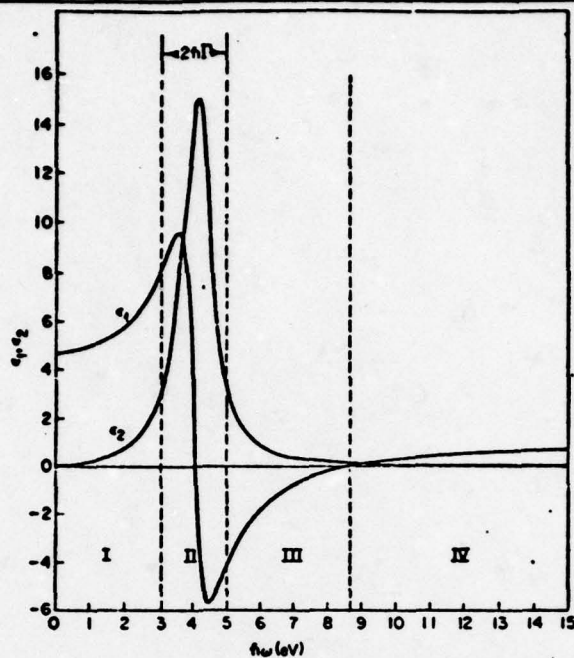
Figure 1
(Ref 8)

Spectral dependence of ε_1 and ε_1. The curves are calculated for the case in which $\hbar\omega_0 = 4$ eV, $\hbar\Gamma = 1$ eV, and $4\pi Ne^2/m = 60$. The onset of region IV is defined by $\varepsilon_1 = 0$.
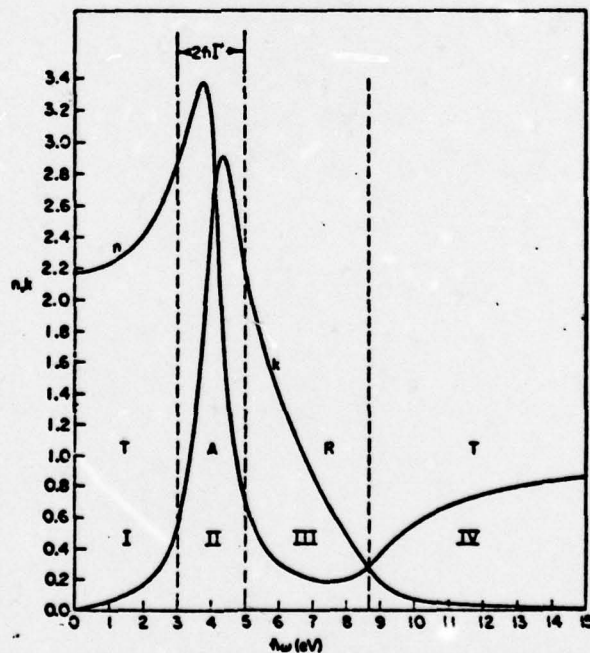

Figure 2
(Ref 8)

Spectral dependence of n and k. The curves are calculated from the values of ε_1 and ε_2 given. The regions I, II, III, and IV can be seen to be primarily transmitting (T), absorbing (A), reflecting (R), and transmitting (T), respectively.
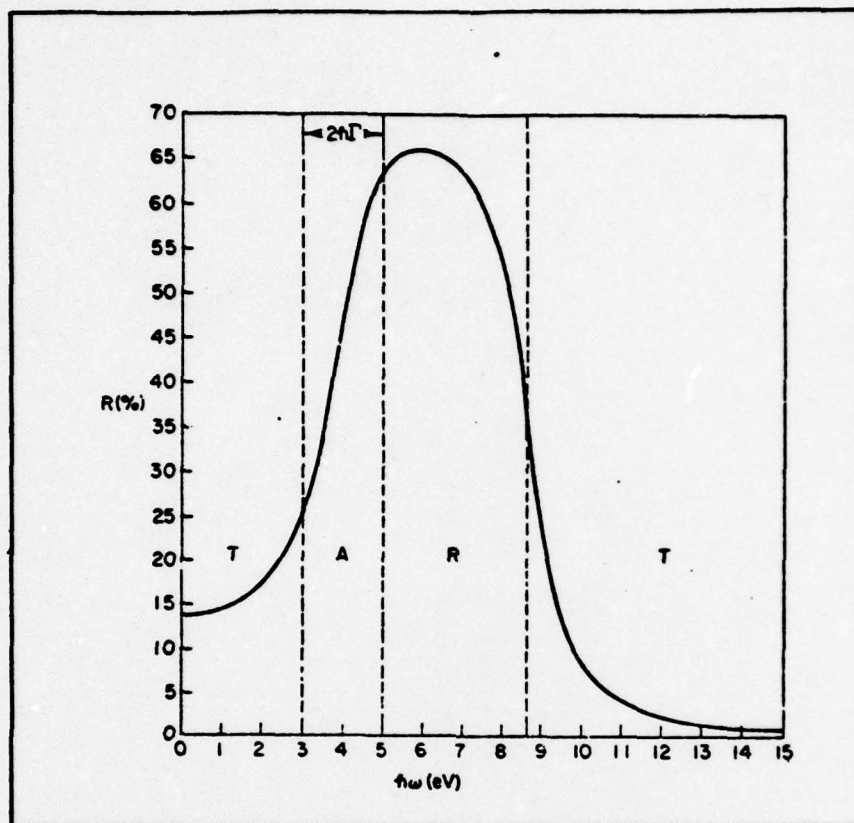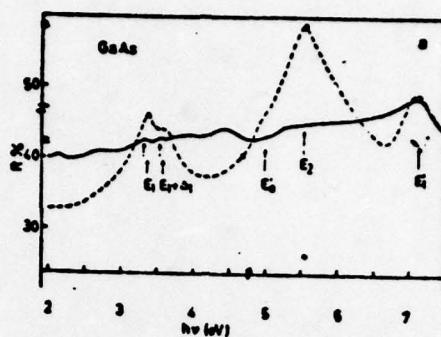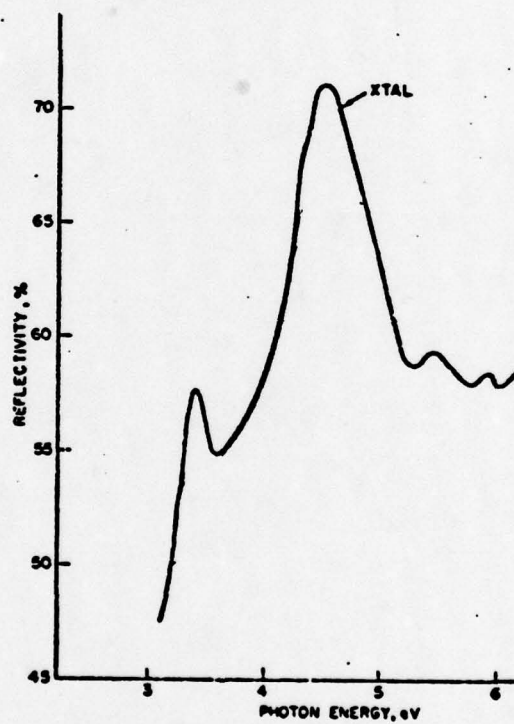
16

Figure 3, Reflectivity vs. Frequency for the
given oscillator (Ref 8)

(a) Reflectivity spectrum of single–crystal (---) and
Te implanted (—) GaAs sample, respectively.

Reflection spectra in the 3–6.5 eV energy range of a
silicon sample

Figure 4, Reflectivity Spectra for crystalline
Si and GaAs.

III Apparatus

Since R is defined as the ratio of the reflected to incident intensities from a surface, it is necessary to be able to measure both I_o and I_r. Furthermore, to avoid the problems associated with the variation of R with angle of incidence, this angle must be small enough so that one can neglect the θ dependence. In this case (near normal incidence) the reflectivity becomes:

$$R \approx \left(\frac{n_1 - n_2}{n_1 + n_2}\right)^2 \tag{31}$$

where n_1 and n_2 are the index of refraction of the surrounding and absorbing medias, respectively. If the angle of incidence is kept below $10°$, this approximation is valid.

The traditional method of measuring $R(\omega)$ over a wide range is to take two spectra, one for I_o and the other for I_r, and do a point by point division to obtain $R(\omega)$. However, a direct readout of $R(\omega)$ would greatly speed up data taking. This could be accomplished if one had a system that could simultaneously measure I_o and I_r, and then electronically divide the signals. The major problem with this approach is the measurement of I_o and I_r. One possible method would involve two detectors, one for I_o and the other for I_r, but this scheme requires that both detectors have exactly identical spectral responses. A better approach would be to use a single detector mode of operation.

I_o and I_r can be measured by a single detector if the incident light beam is chopped. In this method, a highly reflective mirror and the sample are mounted on a spinning disk (Ref 11). As the disk spins, reflected light from the sample and reference mirrors alternately illuminate

19

the detector. Thus the output signal from the detector contains I_o and I_r in an alternating fashion. Thus, to complete the measurement, this output signal must be resolved into its incident and reflected components. This is easily done by the use of two boxcar integrators.

A boxcar integrator is a device composed of two parts, an enabling gate and a signal integrator. The whole system is capable of measuring an input signal for a specified length of time, at a given time, integrating the signal measured, and then producing an output which is the average of the signal for the enabling time. If the input signal is periodic in time, then the boxcar can be used to take several measurements at the same position on the input signal and produce an average value as the output. Thus by adjusting the enabling gate properly, the integrator can be used to sample a given portion of a signal at any point on the signal. As a result, I_o and I_r can be measured by individual boxcars if they are properly enabled (Fig 5).

In order to have a reliable value for I_o, care must be taken in preparing the reference mirror. First, a suitable coating must be chosen. This reflective coating must have a relatively flat reflectance spectrum over the wavelength range in question. Aluminum seems to be the best choice for wavelengths between 200 and 500 nm. Its reflectivity curve varies by only 1% in this region and has a relatively high absolute reflectivity, approximately 92%. However, not only is the proper choice of materials important, but so is the method of deposition of the reflecting film. Too thin of a film will be partially transmissive at lower wavelengths, giving erroneous readings. Thus, for aluminum, a 100 nm thick layer, on glass, is required for an opaque film. The glass surface must be cleaned in an ultrasonic bath of Chromic acid for at least one hour

or the Al will not stick properly. Also, since Al oxidizes rapidly, and 200-250 nm radiation enhances oxidation, a MgF_2 coating of 25-30 nm thickness is needed to preserve the mirror (Ref 12). If these precautions are taken, then an Al film mirror will reflect a suitable reference beam.

A modified version of a reflectometer designed by D. Beaglehole was used for all measurements (Ref 11). Figure 6 details the experimental layout. The Deuterium and tungsten lamps were used to provide the incident light for the monochromator. Although the Deuterium lamp's spectrum is not structureless, any rise in I_o is accompanied by an equal percentage rise in I_r and the ratio of the two remains constant. The tungsten and Deuterium lamps were used to provide light from 450 to 380 nm and from 380 to 210 nm in wavelength, respectively. The monochromator was of the Seya-Namioka mount design, equipped with 650 μm slits and a Bausch and Lomb grating with 1200 grooves/mm and blaze wavelength of 70 nm. The monochromator output was focussed onto the spinning sample disk of the rotary device by the use of mirrors F1 and S1. The rotary device is a trigger mirror and sample holder mounted on an a.c. synchronous motor (Fig 7). The sample holder contains the reference mirror, built as earlier described, and the sample. Mirrors S2 and F2 were used to image the reflected beam from the sample disk onto the photomultiplier tube. The output from the PMT was amplified and shaped by using the Keithley and Molectron amplifiers. The differential integrator combined with the dual pulser makes up the two boxcar integrators. The differential integrator contains two separate integrators and normally produces an output which is the difference between the two. However, for this experiment, the differential integrator was operated as two independent integrators. The dual pulser was used to provide the two enabling pulses for the integrators, thus separately measuring I_o and

21

I_r. The integrated values for I_o and I_r were then divided by the use of the multiplier/divider unit and the ratio, I_r/I_o, was plotted on the X-Y recorder.

A trigger pulse was obtained from a photodiode used to detect a reflected light pulse off of the trigger mirror. The trigger mirror was illuminated by the use of the HeNe laser. The resulting pulse from the photodiode was used to trigger the dual pulser to produce the properly delayed enabling pulses, thus synchronizing the timing of the boxcar integrators with the motor. The timing between the PMT signal and the enabling pulses was monitored on a Hewlett-Packard Model 1220A Oscilloscope.

With this system, a change in $R(\omega)$ of 2% can be detected, and an absolute value for $R(\omega)$ is accurate to ±1%. These values were obtained by taking several spectra of undoped, compensated GaAs crystals. Assuming that the crystals had identical reflectance spectra, the standard deviation of the signal, at 10 nm intervals, for the entire spectral region was computed. Standard deviations of less than 1% in $R(\omega)$ can be obtained for a single crystal for one complete data run. It is this single data run error that is presented on the $R(\omega)$ curves. However, run to run inconsistencies will increase this error to the aforementioned 1%, and must be taken into account when reviewing the data. The main source of noise in this system is instability in the Molectron integrator. Hence, a continuous reflectivity spectrum can be obtained to within an absolute value of ±1%. However, due to the large error, fine structure in $R(\omega)$ is lost, and only the major peaks can be observed.

22

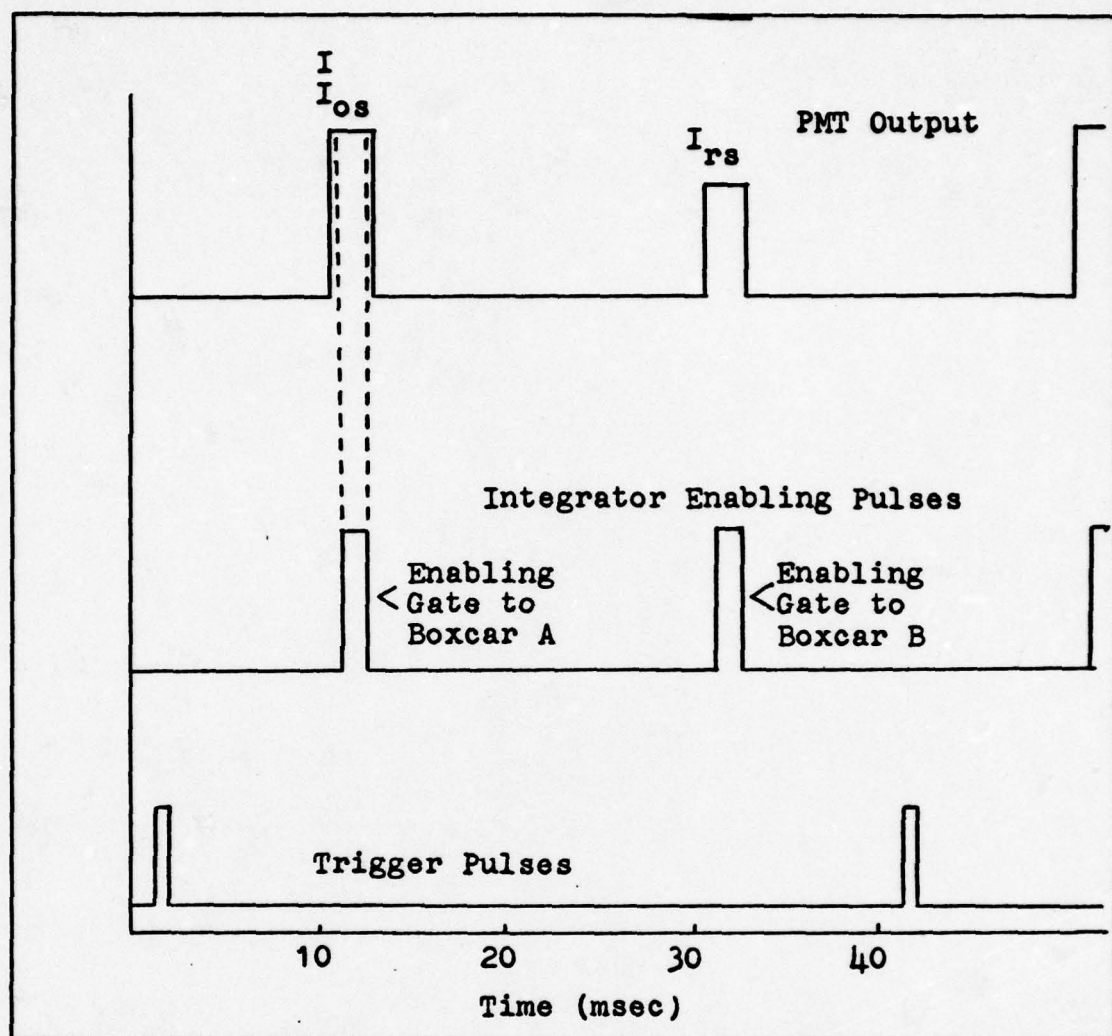Figure 5, Timing of Boxcar Integrators with the
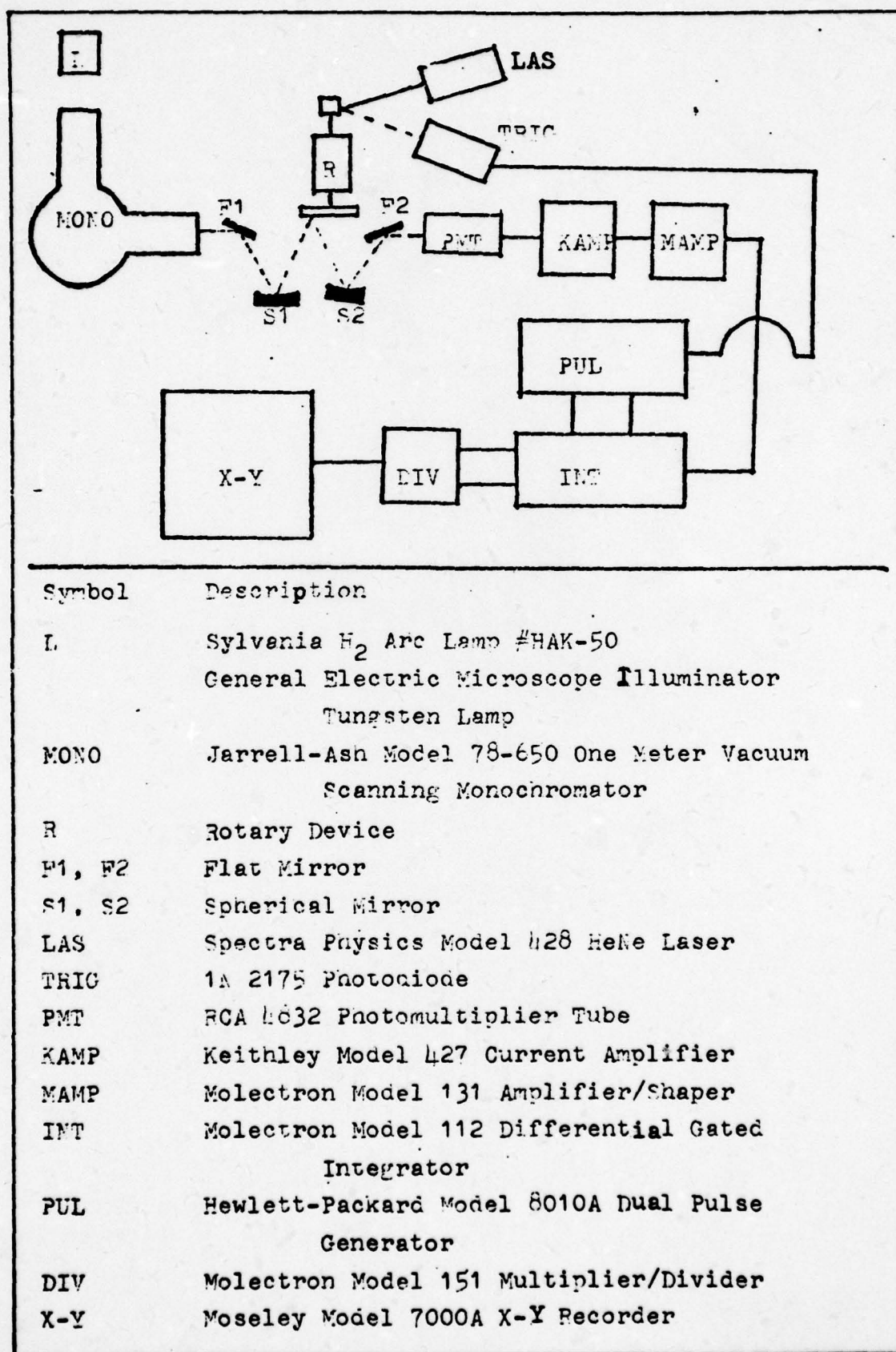Output from the PMT.

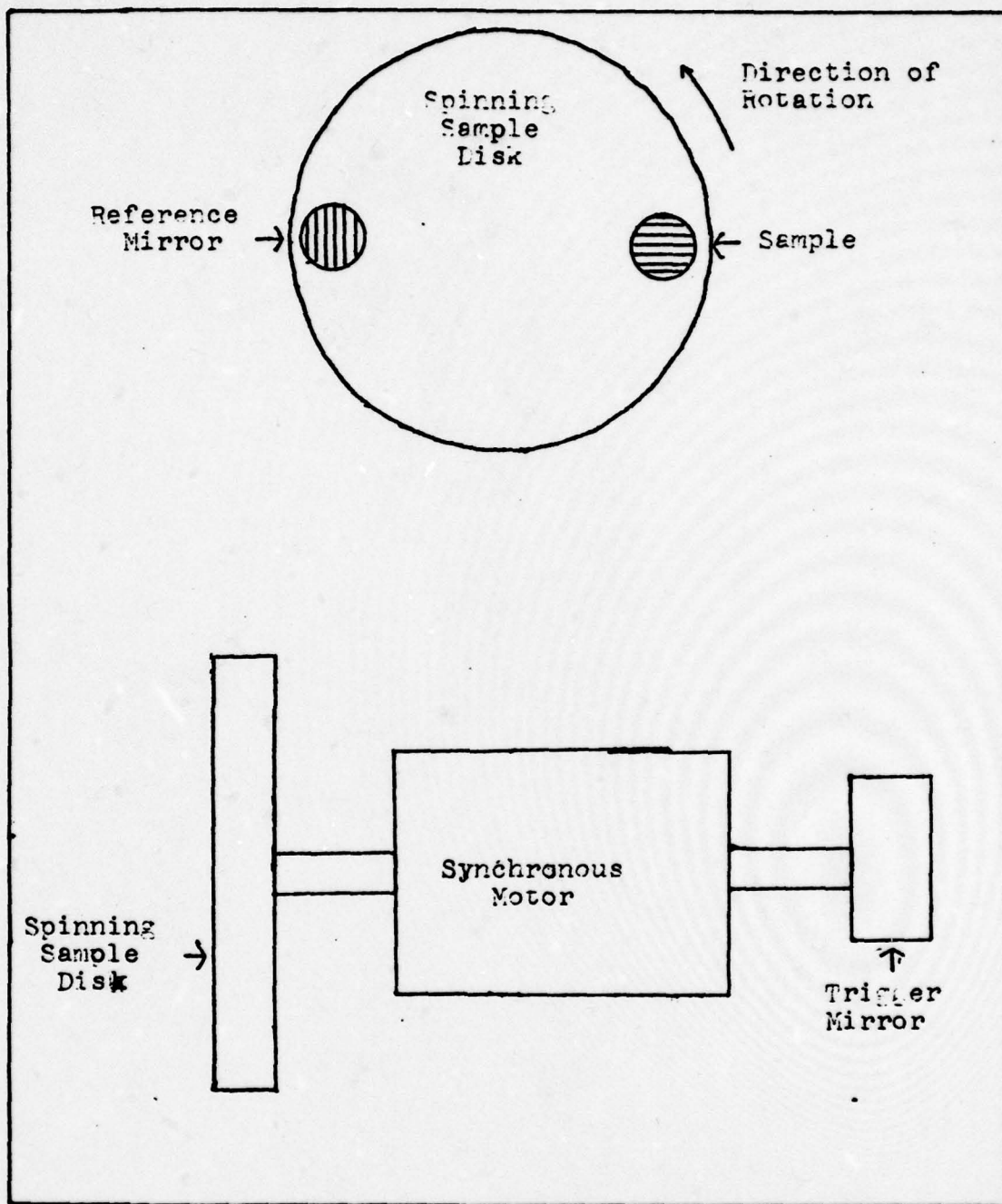| Symbol	Description
L	Sylvania H_2 Arc Lamp #HAK-50
	General Electric Microscope Illuminator Tungsten Lamp
MONO	Jarrell-Ash Model 78-650 One Meter Vacuum Scanning Monochromator
R	Rotary Device
F1, F2	Flat Mirror
S1, S2	Spherical Mirror
LAS	Spectra Physics Model 428 HeNe Laser
TRIG	1N 2175 Photodiode
PMT	RCA 4832 Photomultiplier Tube
KAMP	Keithley Model 427 Current Amplifier
MAMP	Molectron Model 131 Amplifier/Shaper
INT	Molectron Model 112 Differential Gated Integrator
PUL	Hewlett-Packard Model 8010A Dual Pulse Generator
DIV	Molectron Model 151 Multiplier/Divider
X-Y	Moseley Model 7000A X-Y Recorder

Figure 6, Experimental Equipment

24

Figure 7, Rotary Device and Trigger Mirror

IV Procedure

Data Acquisition

Data on $R(\omega)$ was collected in the following manner. The prepared sample was mounted in the sample holder with equal size apertures, 3 mm in diameter, covering the reference mirror and sample. The angle of incidence for I_o was set at 7° and the sample holder was rotated at 25 Hz. The PMT, at a -1250 V, had its dark current suppressed to zero, using the noise suppression on the Keithley amplifier. The dark current, I_{ds}, must be suppressed or it adds to the signal current, I_{os} and I_{rs}, of I_o and I_r, producing erroneous data since

$$R(\omega) = \frac{I_r}{I_o} = \frac{I_{rs}}{I_{os}} \neq \frac{I_{rs}+I_{ds}}{I_{os}+I_{ds}} \tag{32}$$

The Deuterium lamp was positioned at the entrance slit of the monochromator such that the grating was fully illuminated, and the exit beam was centered on the reference mirror and sample aperatures. By monitoring the output from the PMT and the enabling gates on the oscilloscope, these gates were positioned at the peaks of I_{rs} and I_{os}, respectively, for each integrator (Fig 5). A 0.15 msec enabling gate time was used for each integrator, with a 17 msec time delay between the two gates. The RC time constant was equal for both integrators and RC = 10^{-4}. The input signal size to the integrators was limited to

$$1.0V \leq I_{os} < 10.0V \tag{33}$$

where I_{os} is now in volts. If I_{os} is greater than 10.0 V, the integrator will discharge, and when I_{os} is less than 1.0 V, it is below the minimum

signal value for reliable operation of the multiplier/divider unit. Hence, these limits must not be exceeded. Within these operating limits, the output produced by the multiplier/divider unit is proportional to $R(\omega)$. For maximum resolution of $R(\omega)$ the Y axis on the X-Y recorder was adjusted to give a maximum deflection, without pegging, at the maximum value of $R(\omega)$ in the spectrum. The X axis of the X-Y recorder was driven at 1 inch/100 sec and the monochromator was scanned at 10 nm/min, always starting at 210 nm.

Four data runs, from 210 nm to 380 nm, were made consecutively, with the Deuterium lamp. The tungsten lamp was then used to make four data runs from 380 nm to 450 nm, completing the data set, producing a continuous plot of $R(\omega)$ versus wavelength. Care must be taken in positioning the lamps. A change in lamp position changes the position of the monochromator's exit beam on the sample disk, which would result in false readings. Therefore, for run to run consistency, the lamps were repositioned in the same place. For precise wavelength calibration, a tick mark on the $R(\omega)$ curves was produced every 10 nm by the use of an event marker on the monochromator.

Absolute values for $R(\omega)$ at any point on the graph can be obtained if $R(\omega)$ at one point is known and the reflectivity curve of the reference mirror is taken into account. Since it is changes in $R(\omega)$ that we are looking for, not absolute measurements, the reference mirror interaction with $R(\omega)$ will be neglected. This can be done since the change in reflectivity of the reference mirror over the spectral region in question is less than 0.5%, and falls well within the error of the data. Thus, with the reference mirror taken as a standard, $R(\omega)$ at a single point is needed to finish the data run. This is accomplished by shutting off the motor and taking a d.c. measurement of I_{rs} and I_{os}, and taking the proper ratio to

27

give $R(\omega)$. This d.c. measurement of $R(\omega)$ was made at 380 nm for each spectrum, and was taken to be the value of $R(\omega)$ at 380 nm. This value was assigned to the average height of deflection, at 380 nm in the data. Therefore $R(\omega)$ can be obtained at any point on the reflectivity curve since a linear increase in $R(\omega)$ produced a linear increase in the data. The standard deviation in the signal height is reported as the standard deviation in $R(\omega)$.

Even though a continuous reflectance spectrum is produced, only the values for $R(\omega)$ at 10 nm intervals were calculated and plotted. No loss in resolution of $R(\omega)$ was suffered since the size of the error already present in the data obscured any fine structure in $R(\omega)$. After $R(\omega)$ was plotted, the values for D, the degree of damage, were then calculated from the average values at $R(\omega)$ at the proper wavelength. The error in D, as a function of the error in $R(\omega)$, was calculated and found to be $\pm 10\%$.

Laser Annealing

The virgin Si and all GaAs crystal surfaces were grown by the Bridgman method. The implanted Si substrate was an epitaxial layer, grown on a Si base. The GaAs surface was in the (100) orientation and the Si surface was in the (111) plane. The implantation was done at normal incidence to the surface, as was the laser annealing.

The virgin samples were prepared for annealing in the following manner. For GaAs, the crystal was dipped for one minute apiece in HCl, H_2O, a 3:1:1 ratio solution of H_2SO_4: H_2O: H_2O_2 (30%), H_2O, and dehydrated ethanol, in that order, then blown dry. The HCl was used as a surface cleaner, the H_2SO_4 was a strong etch, the H_2O was a wash between solutions, and the ethanol was used so as not to leave a residue film upon drying. The Si was dipped for one minute each in HF (48%), H_2O, and dehydrated

28

ethanol, and then blown dry. The HF was used to clean off the surface layer of SiO_2, and the H_2O and ethanol were used as in GaAs. All baths were at room temperature. This cleaning procedure was found to give the best surface for laser annealing (Ref 13). However, implanted samples were prepared differently from the virgin samples due to uncertainties in the chemical reactions of the implanted layers. Both the implanted GaAs and Si were washed in dehydrated ethanol and blown dry just prior to laser annealing.

Immediately after the sample surface was prepared, the sample was laser annealed. The annealing was done with a Holobeam Q-switched ruby laser. The annealing beam was 30 nsec in length, with λ = 694.0 nm, a beam profile as given in Figure 9, and was symmetric about r = 0. The sample aperture was always positioned over the part of the crystal that was under the portion of the beam denoted by A_s.

Surface Effects

In absolute measurements of $R(\omega)$, surface preparation is of paramount importance. Even looking for changes in $R(\omega)$ is difficult if a surface film is changed somehow. Thus, to determine the effects of laser annealing on surface films, the following procedure was used.

$R(\omega)$ was obtained for a virgin sample of GaAs with no surface preparation and for the same sample after treating the surface in HF (48%), rinsing in H_2O and dehydrated ethanol and blown dry. The reflectance spectrum of the HF cleaned sample had undergone a percentage increase when compared to the untreated sample (Fig 10 and 12). However, the ratio of the peak to valley reflectivities remained constant for both samples, within the error of the spectra. Also, the values of D for both samples

29

were within 0.05 of each other, when taking one sample as the reference crystal and the other as the sample crystal. It was concluded from this that D was a good measure of the crystallinity of a sample and was insensitive to surface films. However, if the thin film present was affected by laser annealing, this could cause problems in the measurements of D.

To check the change of the surface films on D, two virgin GaAs crystals were laser annealed at different energy densities, E_d, one at 0.39 J/cm^2 and the other at 0.69 J/cm^2. $R(\omega)$ was obtained for these two samples both before and after treating the surfaces with HF. $R(\omega)$ for both untreated annealed samples were identical, but had undergone a percentage rise in reflectivity from the untreated unannealed GaAs spectra (Fig 12 and 13). Upon cleaning the samples with HF, their respective reflectance spectra suffered another percentage increase in reflectivity from the untreated spectra. However, both laser annealed spectra were still identical to each other and to that of HF treated, unannealed GaAs (Fig 10 and 11). Degree of damage parameters were calculated for all four spectra. D values for both samples were within 0.1 of each other in both the cleaned and uncleaned cases. The 0.39 J/cm^2 samples' value for D changed by only 0.1 due to cleaning the surface, and the same was true for the 0.69 J/cm^2 sample. Therefore, it was determined that to within a change of 0.1, that D was insensitive to surface films. Also, it was concluded that the surface film on GaAs was not greatly affected by changes in E_d of the annealing beam. Thus, all implanted GaAs samples were not cleaned in HF prior to measuring $R(\omega)$.

The same procedure for virgin Si was followed, with similar results. Virgin unannealed Si cleaned in HF showed a percentage increase in reflectivity over an uncleaned sample. This increase in $R(\omega)$ is due to

30

removal of the SiO_2 layer that forms on the sample when exposed to the atmosphere. Upon laser annealing, virgin Si, all cleaned in HF, showed a percentage drop in $R(\omega)$ over cleaned unannealed Si samples. However, the drop in $R(\omega)$ was constant for all annealing energy densities. $R(\omega)$ for energy densities of 0.95 and 1.48 J/cm^2 were identical (Fig 18 and 19) and their associated degree of damage parameters were within 0.07 of each other. Hence, since Si does form an oxide layer easily, this layer was removed by a HF bath prior to mounting the sample in the system. However, laser annealing at different energy densities showed no change in $R(\omega)$ as a function of E_d. Therefore, prior to mounting in the sample holder, samples of GaAs were not treated with anything, and the Si samples were dipped in a HF bath to remove any SiO_2 formed on the surface.
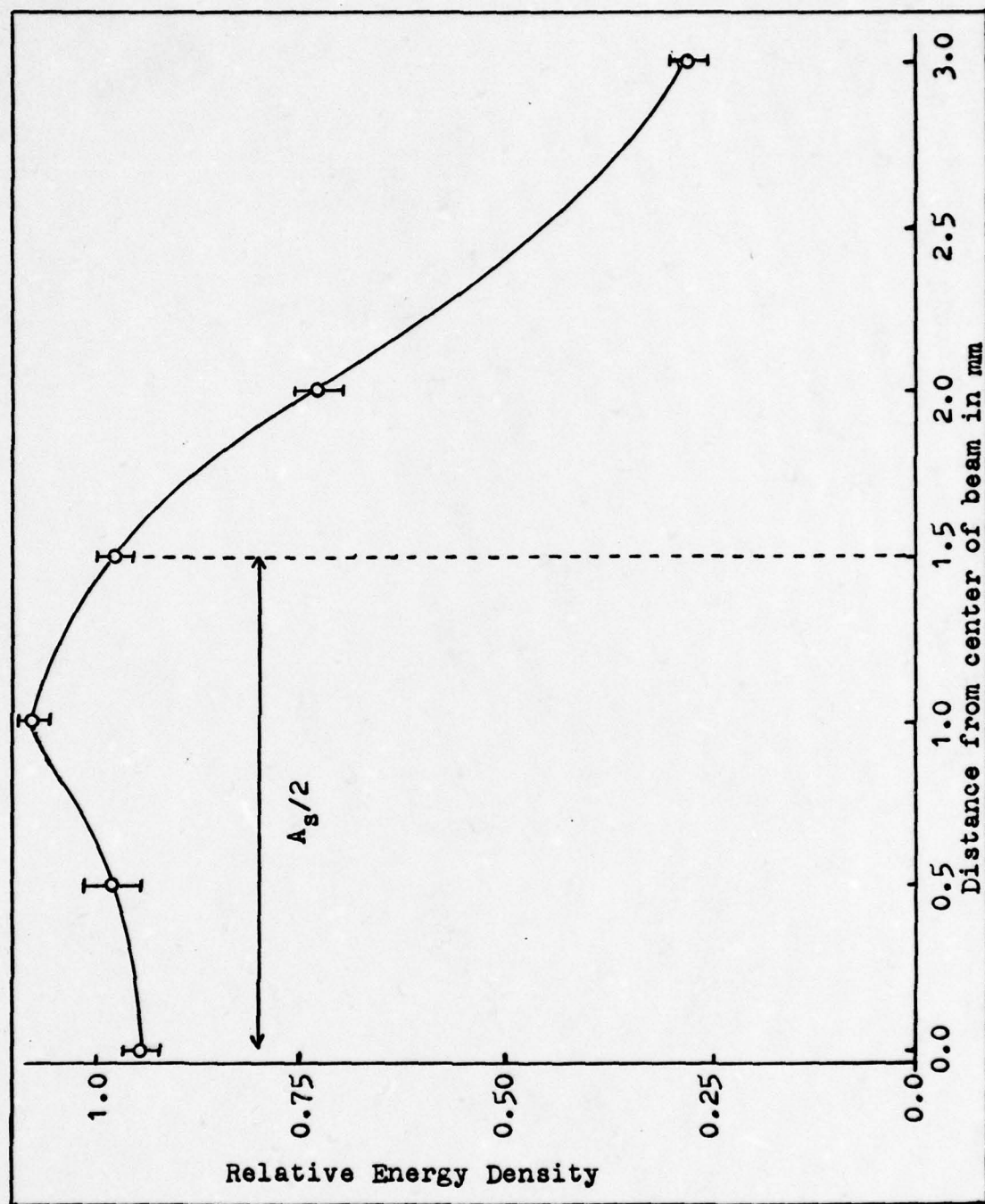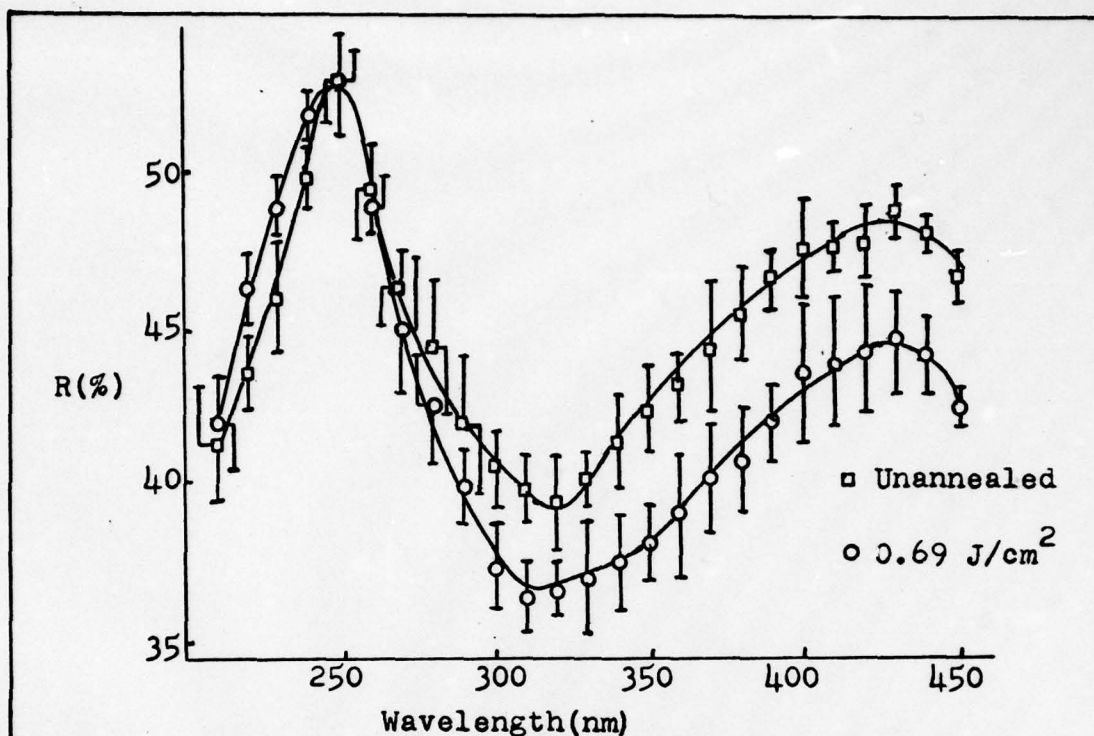
Figure 9, Annealing Laser Beam Profile

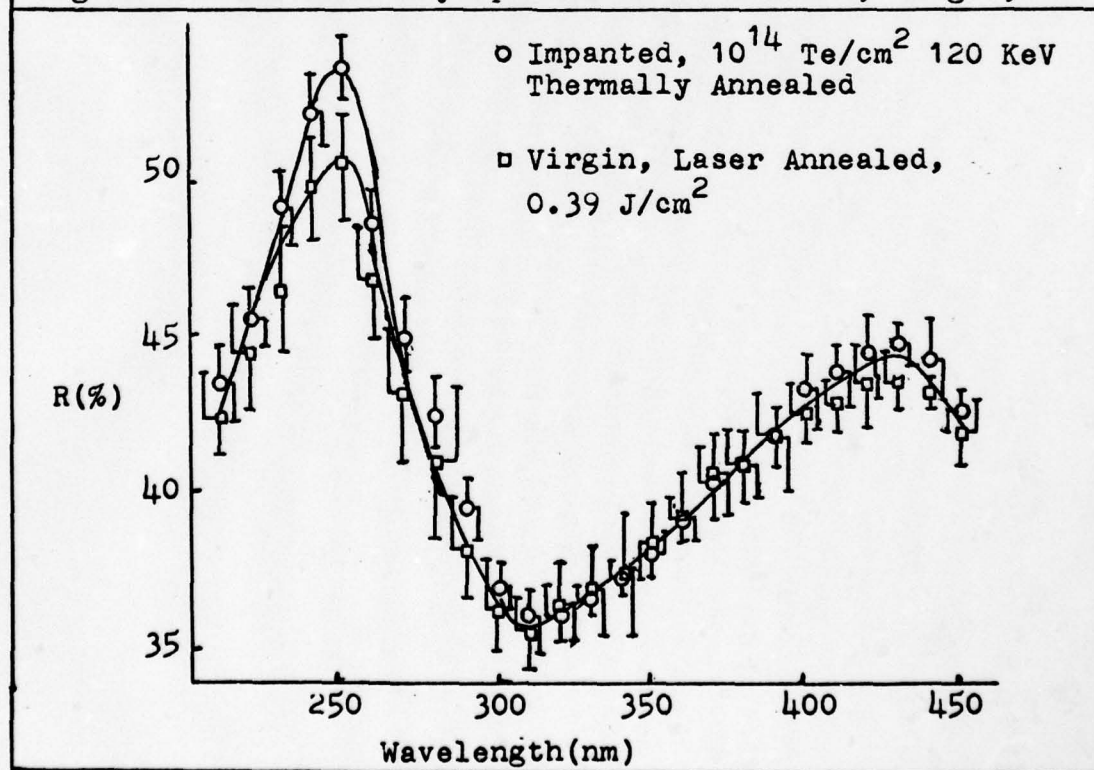Figure 10. Reflectivity spectra of HF cleaned, virgin, GaAs

In the figure: $R(\%)$ axis; Wavelength(nm) axis; legend: □ Unannealed, ○ 0.69 J/cm^2

In the figure: legend: ○ Impanted, 10^{14} Te/cm^2 120 KeV Thermally Annealed; □ Virgin, Laser Annealed, 0.39 J/cm^2; $R(\%)$ axis; Wavelength(nm) axis

Figure 11, Reflectivity spectra of implanted and virgin,

annealed, GaAs.

V Results and Conclusions

Gallium Arsenide

$R(\omega)$ for virgin GaAs, unannealed and uncleaned in HF, is shown in Figure 12, where the error bars represent the standard deviation in the data as described on page 28. Unless otherwise noted, the samples were prepared as described in the previous section. The E_2 peak, at 246.5 nm, is very well defined, however the $E_1 + \Delta_1$ and E_1' peaks, at 400.0 and 275.5 nm respectively, are not resolved. Thus, for convenience, only the E_2 peak and the E_1 peak, at 430.5 nm, shall be referred to in further discussion.

Five virgin samples were annealed at various energy densities to determine the effect of laser annealing on GaAs. The resulting $R(\omega)$ curves provide a reference for what $R(\omega)$ for annealed implanted GaAs should look like, with proper annealing. Energy densities, E_d, of 0.39, 0.51, 0.64, 0.69, and 0.74 J/cm^2 were used. $R(\omega)$ for all samples, except the 0.74 J/cm^2 sample, were identical after annealing. A percentage increase in $R(\omega)$ of these annealed samples, when compared to unannealed GaAs, was observed (Fig 12 and 13). However, upon cleaning the unannealed, 0.39 and 0.69 J/cm^2 samples in HF, their respective $R(\omega)$ values were identical (Fig 10 and 11). $R(\omega)$ for the 0.74 J/cm^2 sample, however, was quite different from the other samples. E_2 was no longer the predominate peak and the absolute value of $R(\omega)$ was greatly reduced. Examination of the surface under a microscope showed extensive cratering in the surface (Ref 13).

A plot of the damage parameter, D, versus E_d, is shown in Figure 22, with the unannealed virgin sample used as the crystalline reference. A

34

slight increase in D is shown for all samples, except for the 0.74 J/cm^2 sample. This increase is approximately a constant for the samples annealed with energy densities of $0.39 \leq E_d \leq 0.69$ J/cm^2, with an average increase of 0.19. The 0.74 J/cm^2 sample suffered a severe increase in D, where D = 0.58. For energy densities between 0.39 and 0.69 J/cm^2, the percentage increase in R(ω) and constant increase in D was not attributed to changes in the crystallinity. Since cleaning in HF showed that the R(ω) curves for annealed and unannealed virgin samples were identical (Fig 10 and 11), the above changes are attributed to a change in the surface film by the laser beam. In the 0.74 J/cm^2 case, however, the very drastic change in R(ω), D, and the cratering of the surface, is attributed to changes in crystallinity, along with a high degree of surface damage. Thus, annealing energy densities of 0.74 J/cm^2 or greater is detrimental to the crystalline surface and should be avoided.

Having established some range of energy densities for annealing, and that within this range laser annealing does not change the crystallinity of a sample, the effect of implantation on R(ω) was studied. Respective R(ω) curves were recorded for three implanted samples at various doses. The dopant was 120 KeV Tellurium ions at fluences of 10^{13}, 10^{14}, and 10^{15} ions/cm^2. Changes in R(ω) with increasing dose is shown in Figure 15. The 10^{13} sample exhibits a nearly virgin R(ω) curve, yet the 10^{14} and 10^{15} samples showed little structure. The values of D for these samples are plotted in Figure 23. It is seen that a sharp increase in D occurs from 10^{13} to 10^{14} ions/cm^2, where the 10^{14} looks to be almost totally amorphous. This is possible since Grasso, et al (Ref 14), found that GaAs was totally amorphous at fluences of 10^{15} ions/cm^2, using 400 KeV Te as the implant. Thus the implanted samples used for laser annealing,

35

120 KeV at 10^{14} Te/cm^2, showed an almost completely amorphous like surface. Thermal annealing of one of these implanted samples returned order to the crystal, as is evident from its reflectivity spectrum (Fig 11). This spectrum is identical to virgin unannealed and laser annealed GaAs. Thus, it was hoped that laser annealing of implanted samples would do the same.

The implanted GaAs was annealed at energy densities of 0.10, 0.17, 0.25, 0.35, 0.48, and 0.68 J/cm^2. $R(\omega)$ for each of these samples is shown in Figures 16 and 17. The start of some regrowth in the implanted layers is evident at the lowest value for E_d by the reappearance of the E_2 peak. The height and definition of E_1 and E_2 are further enhanced by increased energy densities, reaching maximum definition and height at $E_d = 0.35$ J/cm^2 (Fig 17). Further increase in E_d does reorder the crystal, but damage due to the laser starts degrading the surface and reducing $R(\omega)$ when compared to the 0.35 J/cm^2 case (Fig 16 and 17). $R(\omega)$ for the 0.35 J/cm^2 sample shows an E_2 peak that is comparable in absolute and relative peak height to that of virgin GaAs. The E_1 peak in this sample is almost that of virgin GaAs and does have overlapping error bars in many places. Thus, for maximum change in $R(\omega)$, an energy density of approximately 0.35 J/cm^2 is indicated. A plot of D versus E_d for implanted GaAs is shown in Figure 22. It can be seen that a minimum in D occurs from 0.30 to 0.40 J/cm^2. This result is in agreement with previous work on GaAs implanted with 120 KeV Magnesium to doses of 10^{15} ions/cm^2 by Kim, et al (Ref 6). They found that the extinction coefficient, k, and sheet resistivity in implanted GaAs varied with the annealing energy density. A minimum in k was found at about 0.20 J/cm^2, however it took 0.30 J/cm^2 to reduce the sheet resistivity, a value which is in very good agreement with the 0.35

36

J/cm^2 measurement for a minimum D. However, the shape of the D versus E_d curve follows the same pattern as the change in k with E_d, except the minimum in k and D are not at the same value of E_d. At the same time, since the k curves were taken at 632.8 nm and D is for $\lambda = 246.5$ nm, a direct comparison is not appropriate, but a strong indication of a relationship between k and D is concluded.

A comparison of the E_2 peak of the 0.35 J/cm^2 sample with that of laser annealed virgin GaAs shows the peaks to be identical (Fig 13 and 17). If the implanted sample behaves like the virgin samples, then upon cleaning the sample surface with HF, it should have a $R(\omega)$ spectrum that compares with that of HF cleaned virgin and HF cleaned implanted thermally annealed GaAs (Fig 13, 17, and 11). Thus, on the basis of reflectivity, it seems there has been a complete regrowth in the amorphous layers of the implanted GaAs.

However, not only must a regrowth occur, but the dopant must go into substitutional sites. This was investigated by comparing RBS measurements, made at the University of Salford (UK), with $R(\omega)$ and D. Two samples, both implanted with 120 KeV Te at 10^{15} ions/cm^2, were laser annealed, one at 0.35 J/cm^2 for 25 nsec, the other at 0.375 J/cm^2 for 29 nsec. RBS measurements were made on the 0.35 J/cm^2 sample and $R(\omega)$ was measured for the 0.375 J/cm^2 sample. $R(\omega)$ for the 0.375 J/cm^2 sample is quite comparable to that of a 10^{14} sample annealed at 0.25 or 0.48 J/cm^2. Thus, by comparison, the optimum laser annealing conditions were not reached, but a regrowth had occurred. The associated value of D is plotted in Figure 22, and is close to values obtained for virgin annealed samples. RBS measurements of its sister sample shows that the damage had been annealed out, and there is no measurable difference between the laser annealed

37

implanted and a virgin RBS spectra. There was also a substantial reduction in the Te signal, indicating a considerable amount of the dopant had occupied lattice positions (Ref 15). Thus an adequate change in D corresponds to a substantial regrowth in the crystal, with a considerable amount of the dopant occupying regular lattice sites.

Silicon

$R(\omega)$ for virgin, unannealed Si is shown in Figure 18. $R(\omega)$ for Si exhibits two peaks, at 275.5 nm and 364.7 nm, which we will call E_2' and E_1', respectively. As with GaAs, a series of virgin Si samples were laser annealed to determine a reference for the effect of laser annealing. Energy densities of 0.95, 1.175, and 1.48 J/cm^2 were used on virgin Si. $R(\omega)$ for each energy density is plotted in Figure 18 and 19. The structure of all three spectra were identical to within the error of the data, with a percentage decrease in the absolute reflectance spectra when compared to unannealed Si. An energy density higher than 1.48 J/cm^2 could not be obtained from the laser, therefore, no laser damage to the crystal was observed.

A plot of D versus E_d for virgin Si is shown in Figure 24. An almost constant increase in D, due to laser annealing, is observed, with an average increase of 0.08. This drop in absolute reflectivity and slight increase in D is not attributed to a change in crystallinity. A change in surface film is also unlikely, since annealing should reduce any such film, raising $R(\omega)$, yet $R(\omega)$ dropped. The changes in $R(\omega)$ are attributed to changes in the surface smoothness. That is, the one highly polished, flat, surface of the unannealed Si has recrystallized, with slight surface irregularities after annealing. Thus, it was

38

concluded that laser annealing had no adverse effects on the crystallinity of the sample and that the damage threshold for virgin Si could not be reached with the given laser arrangement.

A plot of changes in $R(\omega)$ versus implant dose was not obtained, due to lack of samples. However, Miyao, et al (Ref 2), shows a plot of D versus dose for Si implanted with 50 KeV Phosphorous ions. He shows that D increases linearly with increasing dose up to a fluence of 6×10^{14} ions/cm^2, where the surface becomes completely amorphous. $R(\omega)$ for an unannealed sample is shown in Figure 20. The two peaks present in this spectrum do not correspond to either E_1' or E_2' of Si.

The implanted Si was annealed at four energy densities, 0.51, 0.64, 0.95, and 1.34 J/cm^2. $R(\omega)$ for the 0.51 J/cm^2 sample shows the beginning of order in the crystal by the appearance of the E_2' peak, and the E_1' peak can be regained by increasing E_d to 0.64 J/cm^2 (Fig 21). Raising E_d further shows an increase in the definition and relative peak height of both E_1' and E_2'. However, the decrease in the absolute values in $R(\omega)$ with increases in E_d is not expected and cannot be explained at this time (Fig 20).

A plot of D versus E_d is shown for the implanted Si in Figure 24. From this plot, it is seen that the onset of annealing is at $E_d \sim 0.51$ J/cm^2. D continues to drop with increasing energy density out to $E_d = 1.34$ J/cm^2, indicating that the best annealing conditions have not been met. By extrapolation of this curve, it appears that the best anneal could occur at $E_d \sim 1.6$ J/cm^2, well beyond the capabilities of the laser arrangement used.

RBS measurements, made at the University of Salford (UK), of an identically implanted Si sample, annealed with a 25 nsec, 1.02 J/cm^2

ruby laser beam, shows that the damage has been annealed out (Ref 15).
It is also observed that, within the depth in the crystal measured by
RBS, the remaining In in the crystal has gone in substitutionally (Ref
15). Kurnaev, et al (Ref 4), shows that RBS measurements of (111) Si,
implanted with 90 KeV In to fluences of 5×10^{14}, has been completely
annealed with a 35 nsec, 0.875 J/cm^2 ruby laser pulse. He also reports
that at least 60% of the implants occupy regular lattice sites. Thus, a
considerable regrowth in the implanted layers of Si is indicated by a
substantial drop in D and confirmed by RBS measurements at like energy
densities.

Unfortunately, the laser annealing process does not seem to have
the same effect on the implanted Si as does thermal annealing. Thermal
annealing of Sb implanted Si, at doses of 2×10^{15} at 40 KeV, shows an
increase not only in relative, but also absolute, reflectivity, with
increases in annealing temperature (Ref 3). However, this might not be
a valid comparison, due to problems in measuring the absolute values.
Thus, the degree of damage curves should be further developed.

In conclusion, implanted GaAs and Si undergo a considerable regrowth
in the amorphous layers due to laser annealing. Using a minimum of D as
the reference for best annealing energy densities, GaAs is best annealed
at $E_d \sim 0.35$ J/cm^2. Indications are that Si will reach its best anneal at
$E_d \sim 1.6$ J/cm^2. Also, the energy density of best anneal for GaAs is in the
same vicinity as that for reduction of sheet resistivity. In both Si and
GaAs, RBS measurements confirm that the damage has been annealed out with
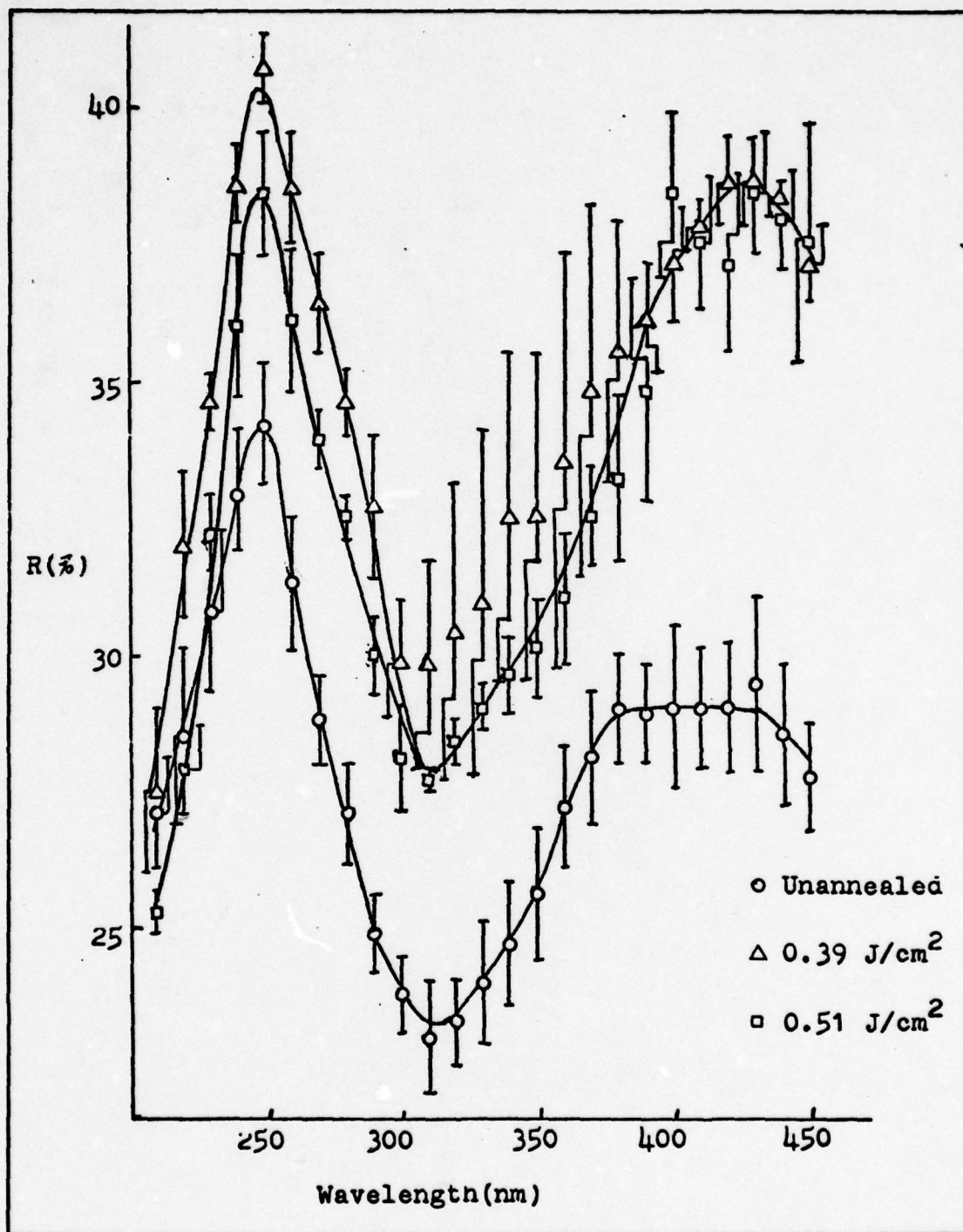approximately the same energy densities it takes to considerably reduce D.

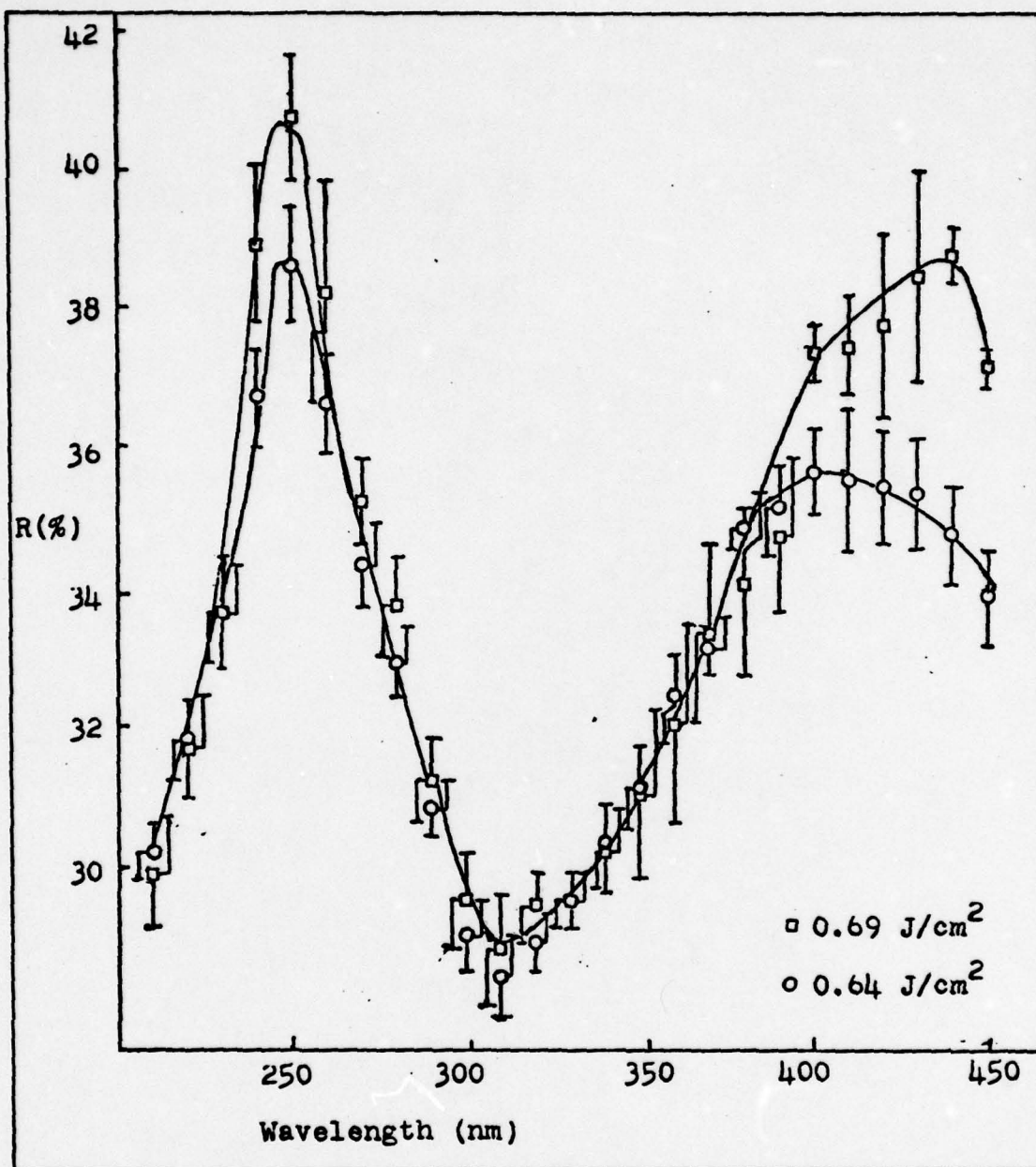Figure 12, Reflectivity Spectra for Virgin, Laser Annealed
GaAs.

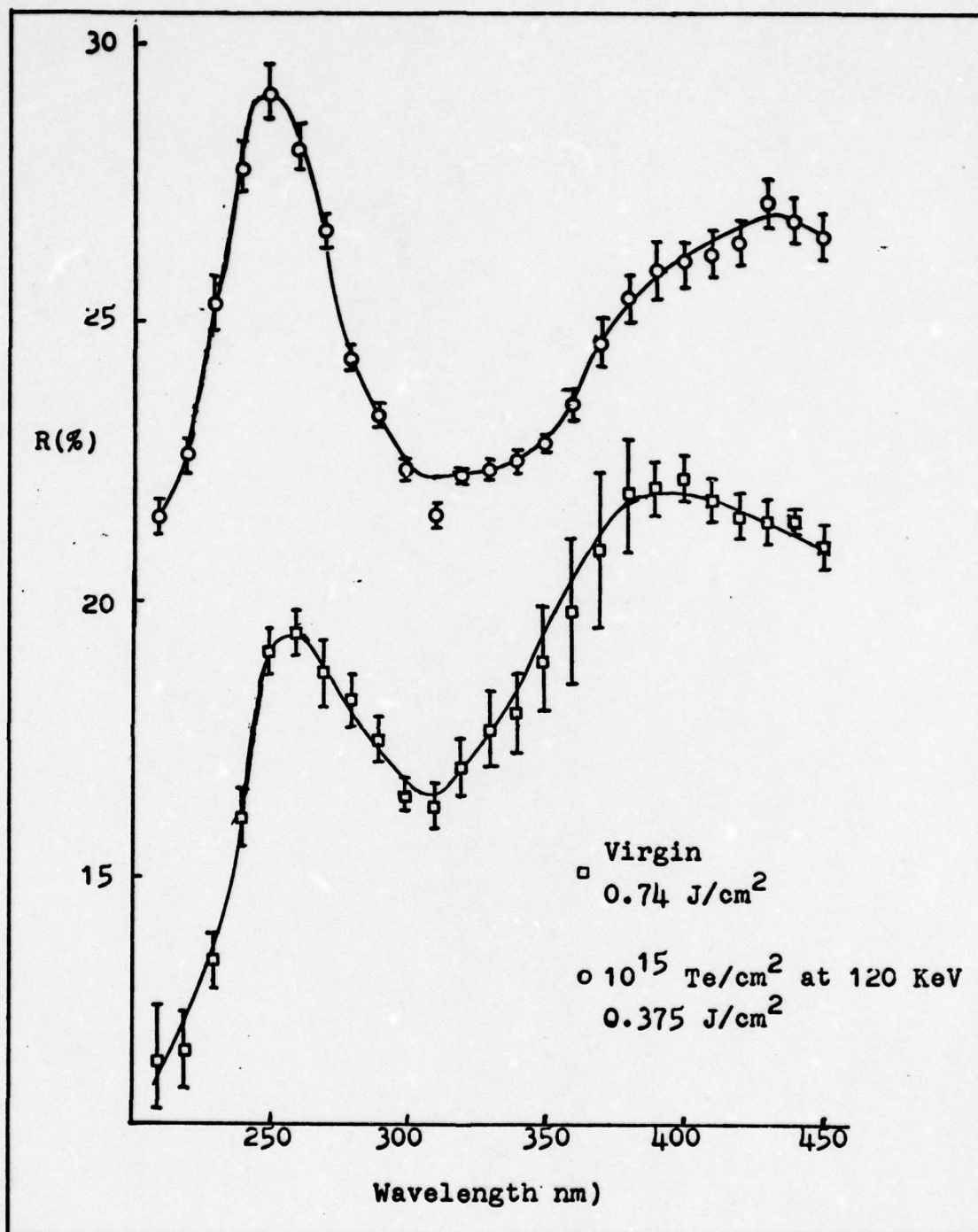Figure 13. Reflectivity Spectra of Virgin, Laser Annealed GaAs.

Figure 14, Reflectivity Spectra for Virgin and
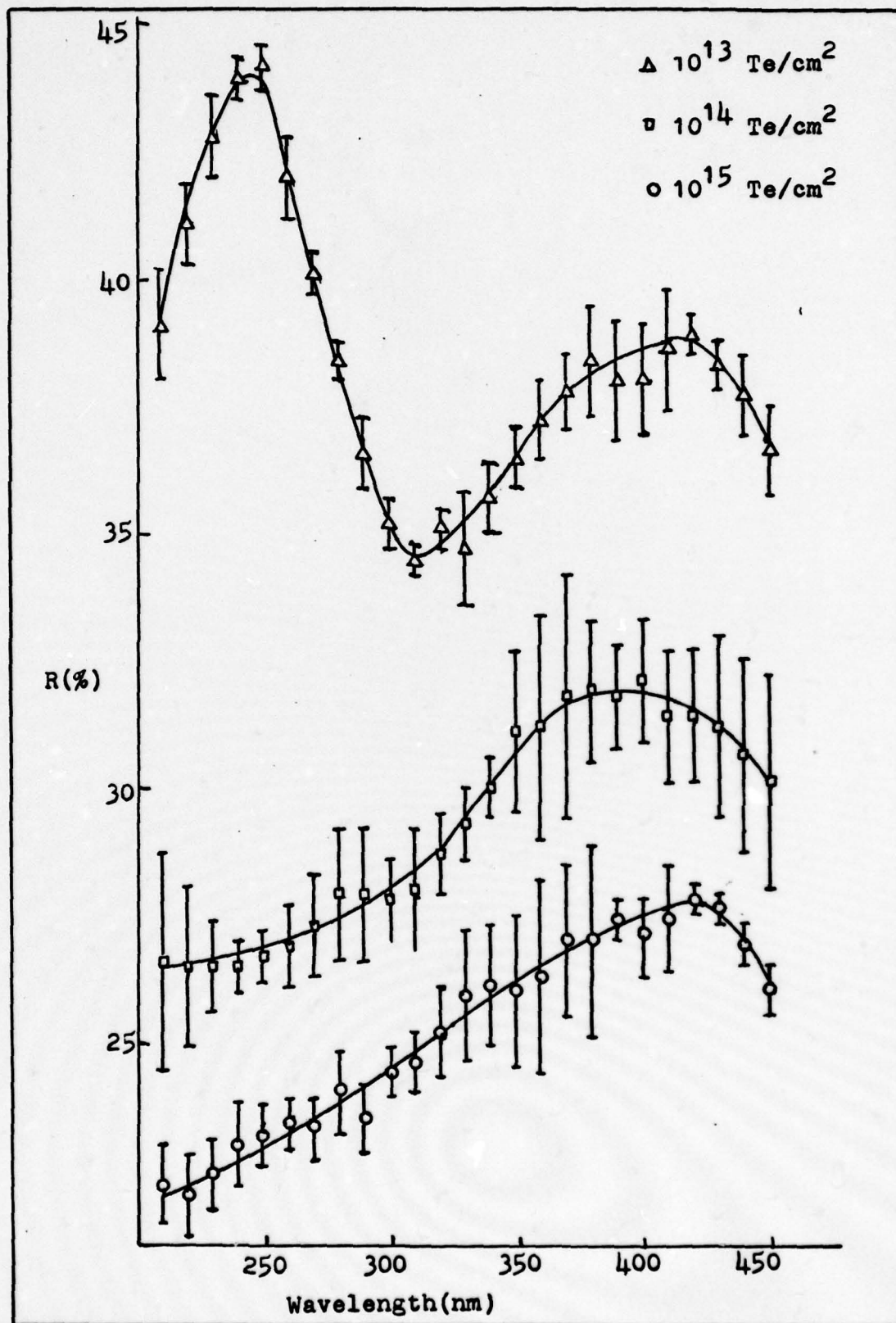Implanted, Laser Annealed GaAs.

43

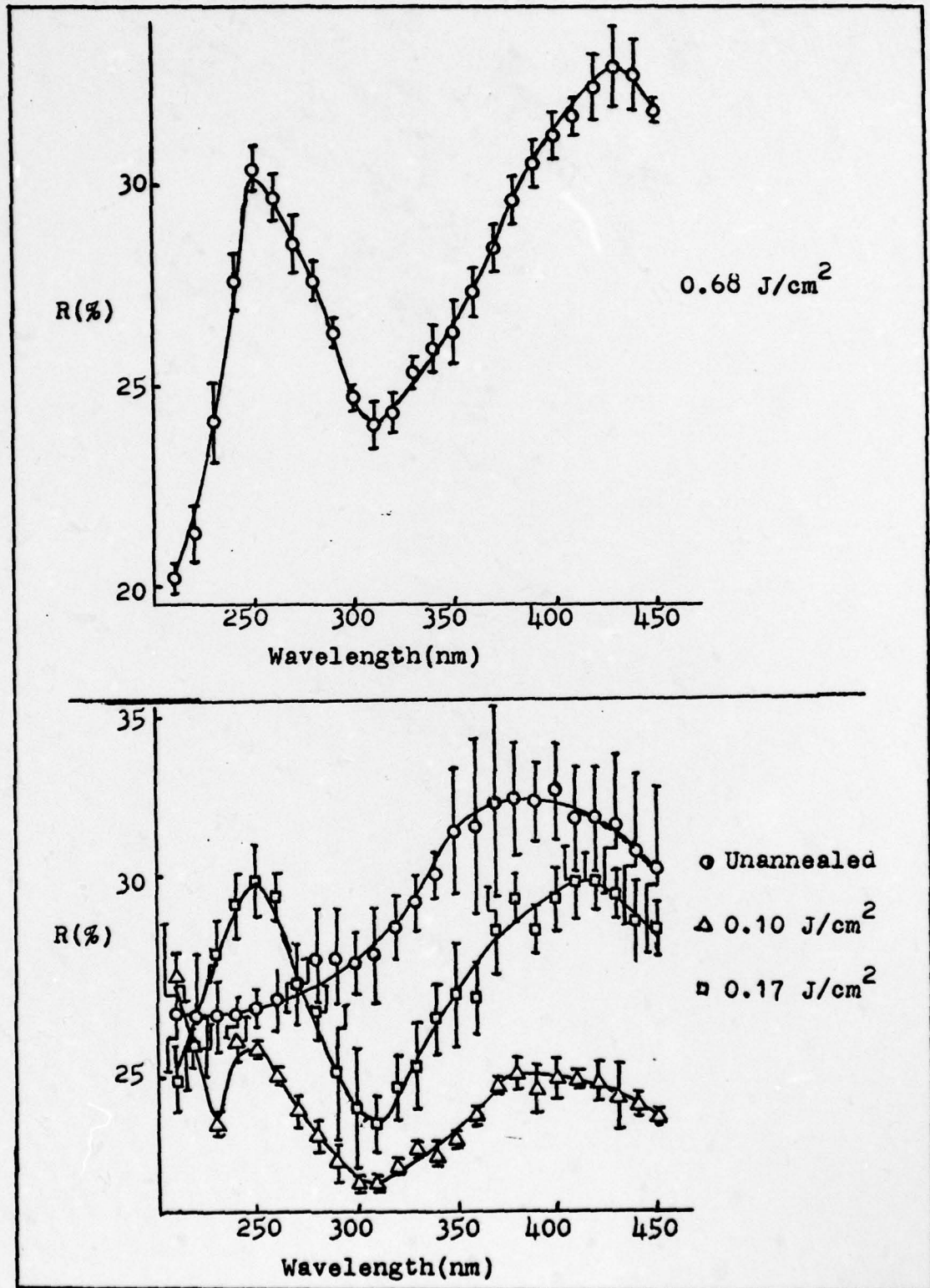Figure 15, Reflectivity spectra for implanted GaAs.

44

Figure 16, Reflectivity spectra of unannealed and
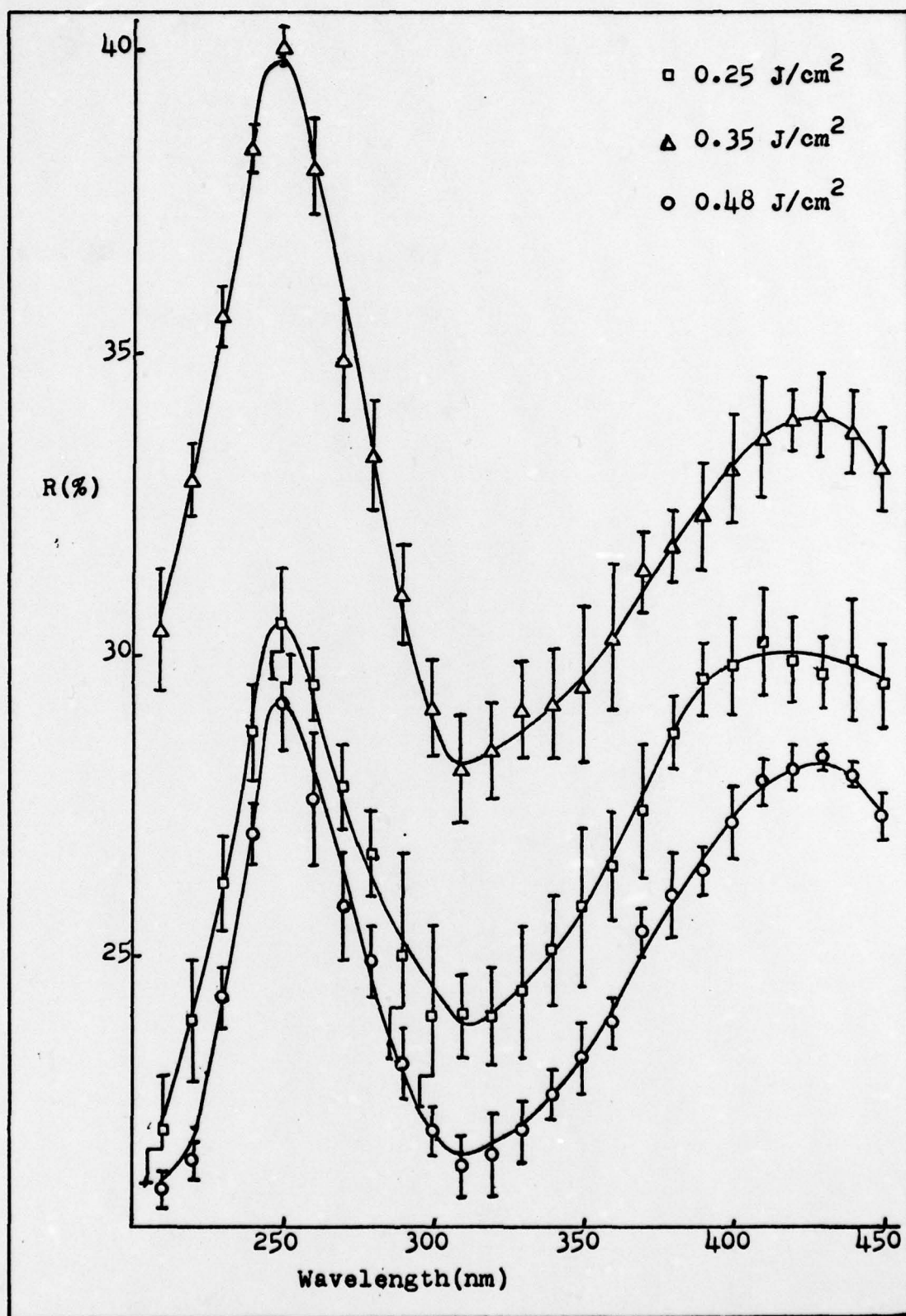laser annealed, implanted GaAs.

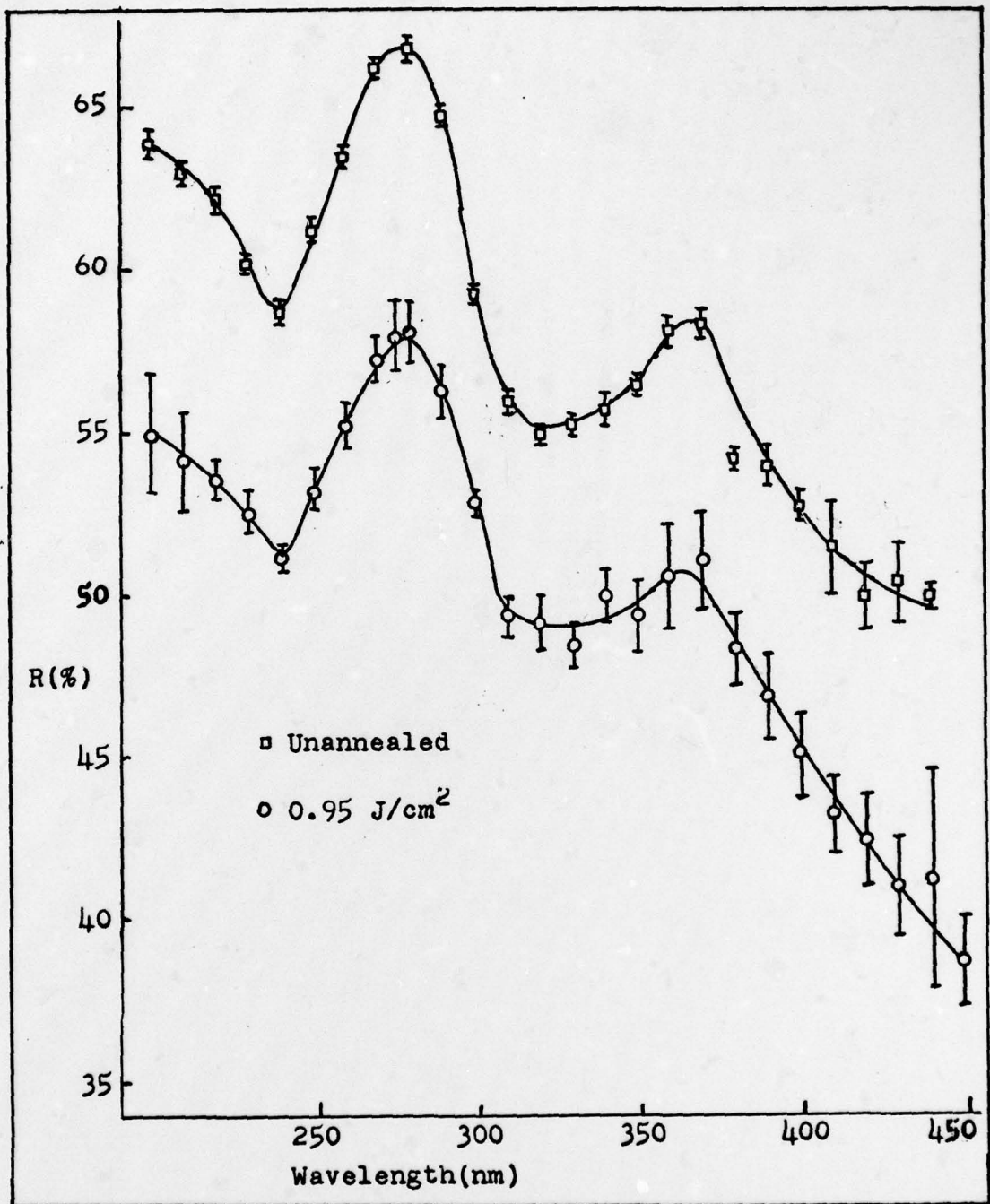Figure 17, Reflectivity spectra of laser annealed, implanted GaAs.

46

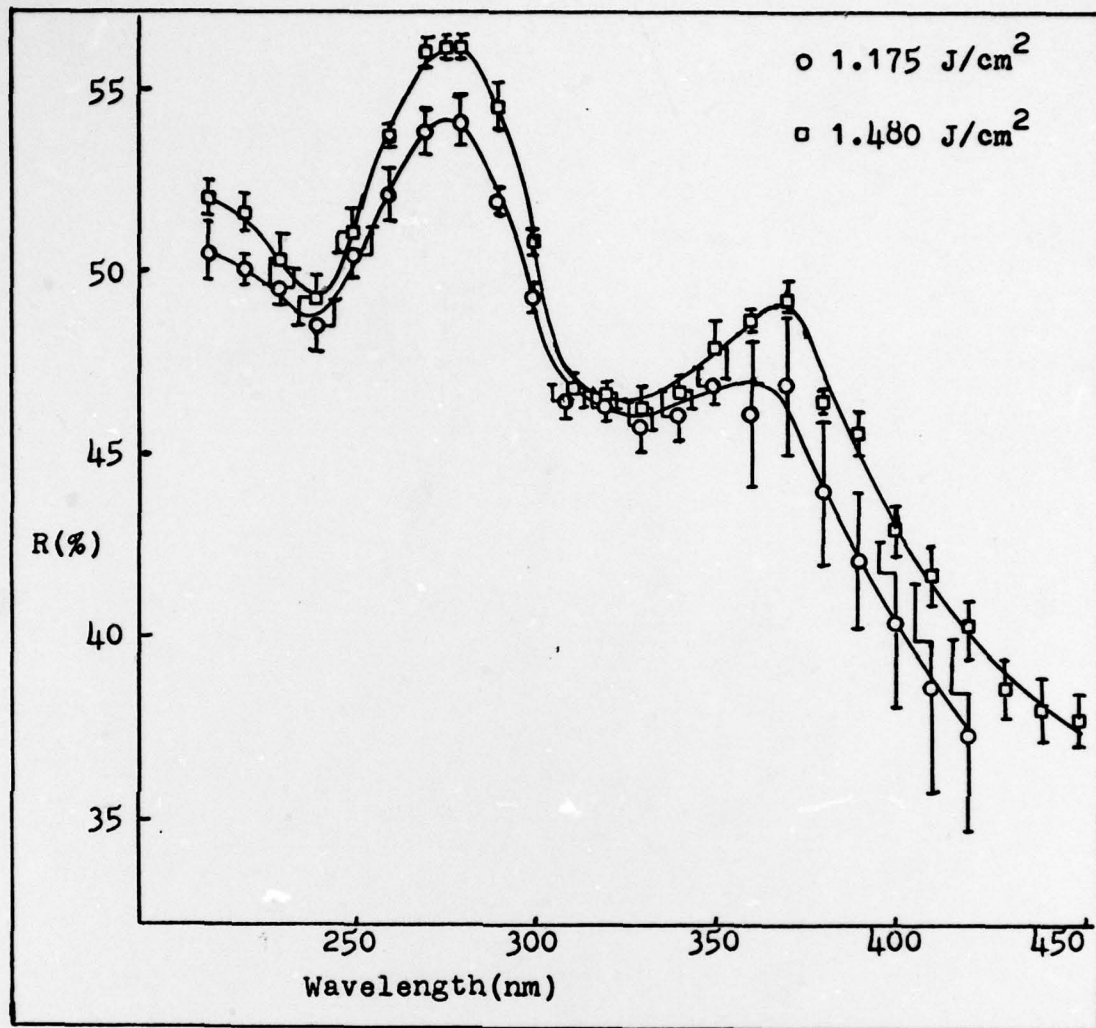Figure 18, Reflectivity spectra for unannealed and laser annealed, virgin Si.

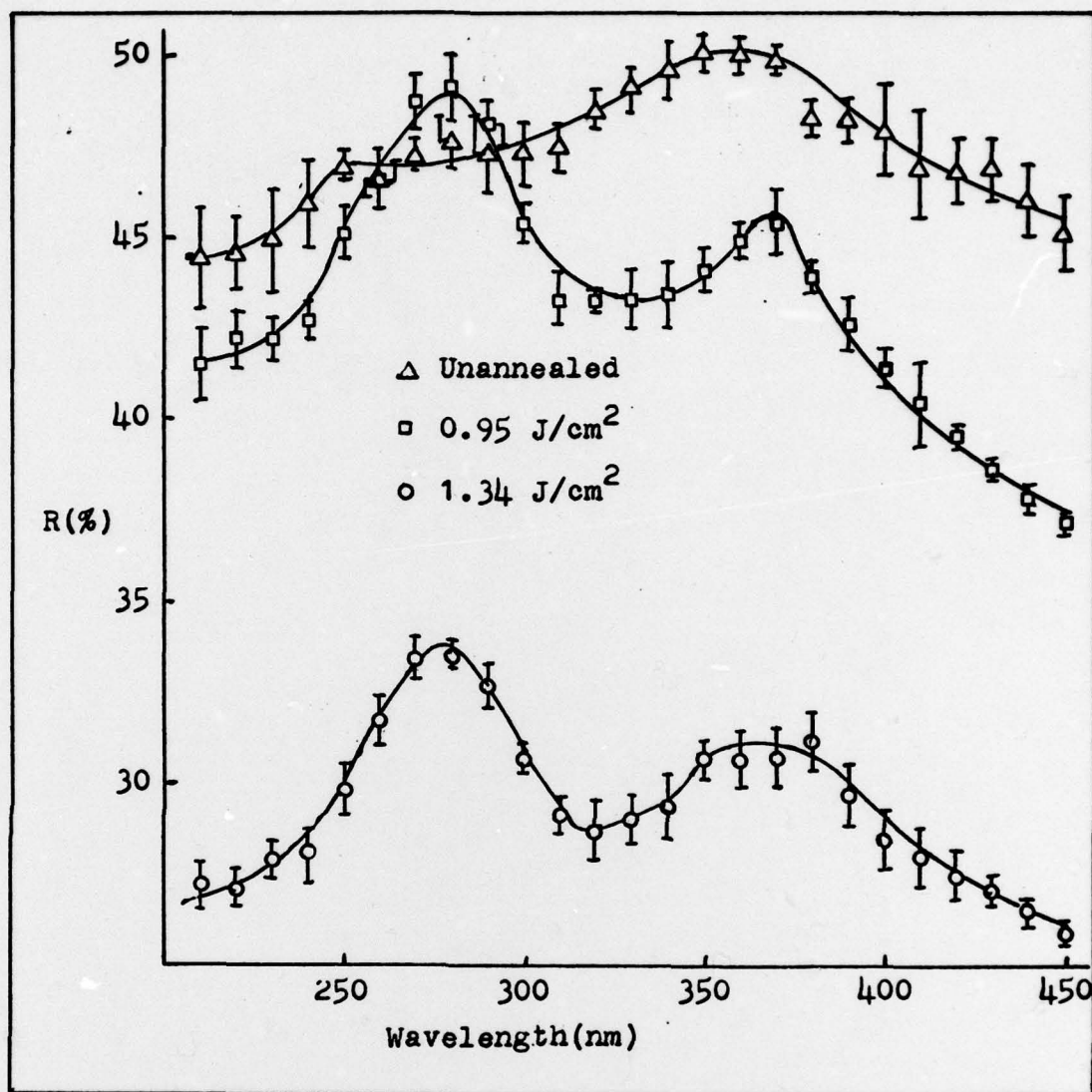Figure 19, Reflectivity spectra of laser annealed,
virgin Si.

48

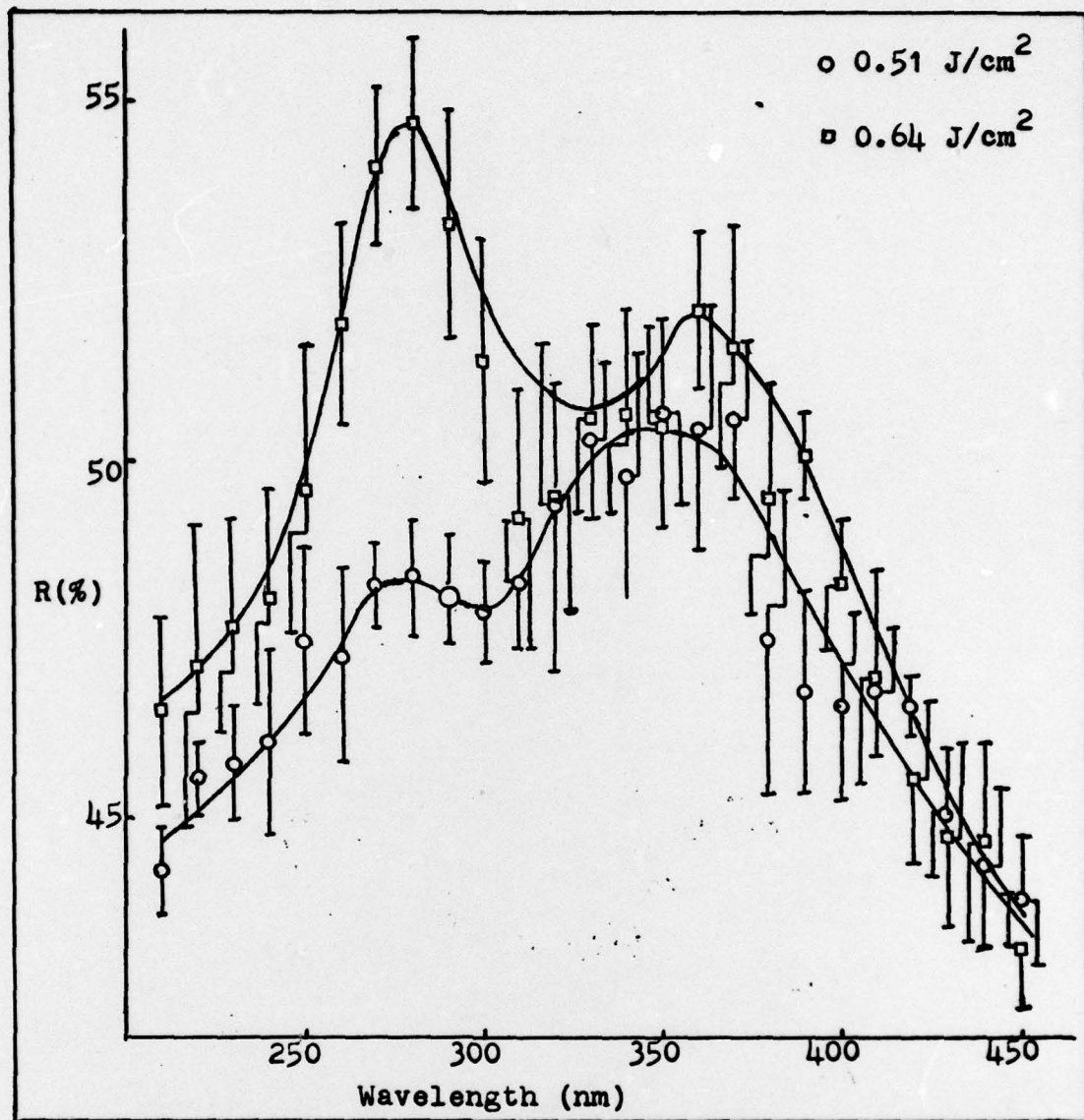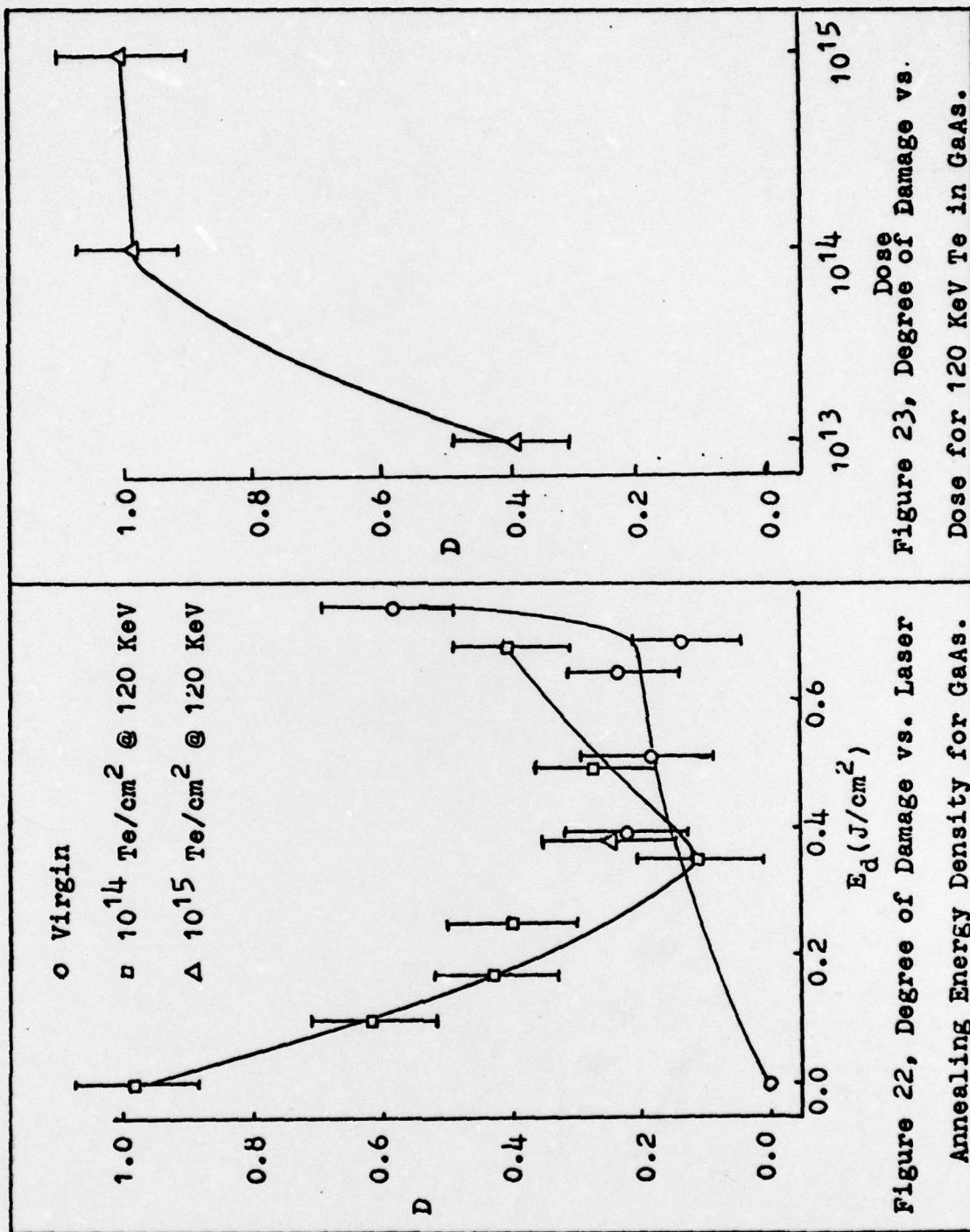Figure 20, Reflectivity spectra of unannealed and laser annealed, implanted Si.

Figure 21, Reflectivity spectra for implanted, laser annealed Si.

Figure 23, Degree of Damage vs. Dose for 120 KeV Te in GaAs.

Figure 22, Degree of Damage vs. Laser Annealing Energy Density for GaAs.
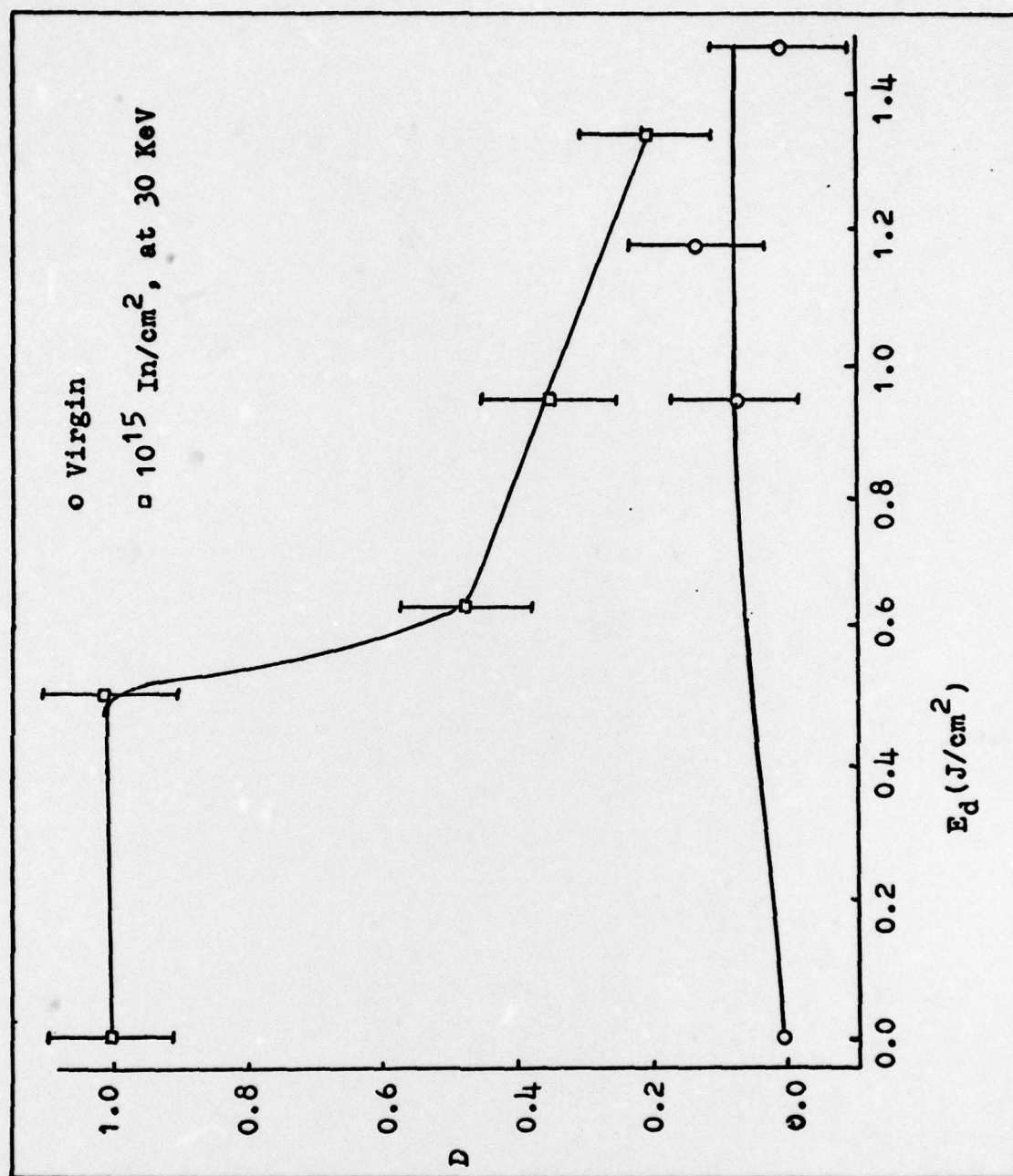
51

Figure 24, Degree of Damage vs. Laser Annealing
Energy Density for Si.

VI Recommendations

The results of this thesis on annealing characterization are encouraging. It would seem that optical reflectivity is a good measure of the crystallinity of the surface layers of an implanted crystal. However, the results are not fully conclusive. The $R(\omega)$ curves presented are for a single crystal at the given annealing energy density. A more reliable set of curves should be obtained by studying at least three different samples annealed at the same energy density. Also, more energy densities should be used, especially at the lower energy settings, to complete the degree of damage curves. The above measurements would be enhanced by a reduction in the signal noise and true absolute value measurements. This requires a change in the equipment.

As for the equipment, two modifications should be made. First, the noise in the integrators should be reduced. The easiest method of accomplishing this is by replacing the Molectron unit with two complete boxcars that are identical to each other, such as two Keithley or PAR boxcars. Secondly, the optical path should be modified to include the reference mirror interaction in both I_o and I_r. With this modification, true absolute measurements of $R(\omega)$ can be obtained with a larger signal to noise ratio.

Other studies to measure values related to the reflectivity are indicated for implanted semiconductors. The indicated formation of an irregular surface on laser annealed virgin samples, by the drop in the absolute value in $R(\omega)$, implies that an experiment to investigate this behavior be pursued. A measure of the surface flatness by a Focault test, or an interferogram, could show if surface flatness is affected by

laser annealing. It was also noted that D, as a function of E_d, assumed the same shape as the k versus E_d curve, except their respective minimum did not coincide. However, the ellipsometry measurements were made at 632.8 nm and the D curves were for λ = 246.5 nm. Hence, there is the need to measure the change in k as a function of E_d at λ = 246.5 nm to confirm or disprove this theory. The rather large changes in D, as a function of E_d, also show that this method could possibly be a better measure of damage profiling than previous measurements. Therefore, taking R(ω) of a sample at various depths in the crystal, by etching the surface, could be used to profile the implantation damage and the subsequent regrowth caused by laser annealing.

53

Bibliography

1. Smith, Bernard. *Ion Implantation Range Data for Silicon and Germanium Device Technologies*. London: Research Studies Press Inc., 1977.

2. Miyao, Masanobu; Miyazaki, Takao; Tokuyama, Takashi. "Optical Reflectivity Studies of Damage in Ion Implanted Silicon," *Japanese Journal of Applied Physics*, 17 (5): 955-6 (1978).

3. McGill, T.C.; Kurtin, S.L.; Shifrin, G.A. "Optical Reflection Studies of Damage in Ion Implanted Silicon," *Journal of Applied Physics*, 41 (1): 246-251 (January 1970).

4. Kurnaev, S. and Uggerhøj, E. "Laser Annealing of Indium-Implanted Silicon," *Radiation Effects*, 40: 91-94.

5. Mason, Robert S. *Laser Annealing of Ion Implanted Gallium Arsenide*. MS thesis. Wright-Patterson AFB, Ohio: Air Force Institute of Technology, December 1978. (AFIT/GEO/PH/78D-3).

6. Kim, Quiesup; Park, Y.S.; Mason, R.S.; Luke, T.E.; Hengehold, R.L.; Yeo, Y.K. "Laser Annealing of Ion Implanted GaAs," *American Institute of Physics Conference Procedings*, Volume 50, 597-602, 1978.

7. Marion, Jerry B. *Classical Electromagnetic Radiation*, New York: Academic Press, 1972.

8. Wooten, Frederick. *Optical Properties of Solids*, New York: Academic Press, 1972.

9. Yariv, Amnon. *Introduction to Optical Electronics* (Second Edition). New York: Holt, Rinehart and Winston, 1976.

10. Dewitt, John Sherman. *Optical Properties of CdSe and ZnO Single Crystals*. MS thesis. Wright-Patterson AFB, Ohio: Air Force Institute of Technology, 1965. (SP/PH/65-8).

11. Beaglehole, D. "A Sensitive Single Beam Device for Continuous Reflectance or Transmittance Measurements," *Applied Optics*, 7 (11): 2218-20 (November 1968).

12. Anders, Hugo. *Thin Films in Optics*, London: Focal Press, 1967.

13. Bradley, Kenneth. *Laser Anneal of and Laser Interaction of Ion Implanted Semiconducting Materials*. MS thesis. Wright-Patterson AFB, Ohio: Air Force Institute of Technology, December 1979. (AFIT/GEP/PH/79D-1).

14. Grasso, V.; Mondio, G.; Saitta, G.; Campisano, S.U.; Foti, G.; Rimini, E. "Optical Reflectivity of Ion-Implanted Amorphous GaAs," *Applied Physics Letters*, 33 (7), (1 October 1978).

15. Christodoulides, Chris. Professor of Electrical Engineering, University of Salford. (Personal correspondence with P. M. Hemenger of the Air Force Materials Laboratory, WPAFB, Ohio) 21 February 1979.

VITA

Bill W. Mullins was born on 17 March 1955 in Lubbock, Texas. He graduated from Cooper High School in Abilene, Texas, in 1973 and attended Angelo State University from which he received the degree of Bachelor of Science in Physics in May, 1978. Upon graduation, he received a commission in the USAF through the ROTC program. He was immediately ordered to active duty at Wright-Patterson AFB, Ohio, as a full time student in the School of Engineering, Air Force Institute of Technology, in June 1978.

Permanent address: 2352 South 33rd
                    Abilene, Texas   79605

REPORT DOCUMENTATION PAGE	READ INSTRUCTIONS BEFORE COMPLETING FORM

1. REPORT NUMBER AFIT/GEP/PH/79D-6	2. GOVT ACCESSION NO.	3. RECIPIENT'S CATALOG NUMBER

4. TITLE (and Subtitle) CHARACTERIZATION OF LASER ANNEALING OF ION IMPLANTED GALLIUM ARSENIDE AND SILICON USING OPTICAL REFLECTIVITY	5. TYPE OF REPORT & PERIOD COVERED MS Thesis
	6. PERFORMING ORG. REPORT NUMBER

7. AUTHOR(s) Bill W. Mullins 2Lt USAF	8. CONTRACT OR GRANT NUMBER(s)

9. PERFORMING ORGANIZATION NAME AND ADDRESS	10. PROGRAM ELEMENT, PROJECT, TASK AREA & WORK UNIT NUMBERS

11. CONTROLLING OFFICE NAME AND ADDRESS	12. REPORT DATE December 1979
	13. NUMBER OF PAGES ~~58~~ 64

14. MONITORING AGENCY NAME & ADDRESS(if different from Controlling Office)	15. SECURITY CLASS. (of this report) Unclassified
	15a. DECLASSIFICATION/DOWNGRADING SCHEDULE N/A

16. DISTRIBUTION STATEMENT (of this Report)

Approved for public release; distribution unlimited.

17. DISTRIBUTION STATEMENT (of the abstract entered in Block 20, if different from Report)

19. KEY WORDS (Continue on reverse side if necessary and identify by block number)
Laser Annealing, Ion Implantation, Gallium Arsenide, Silicon, Optical Reflectivity

20. ABSTRACT (Continue on reverse side if necessary and identify by block number)

The effect of laser annealing on ion implanted GaAs and Si has been assessed using optical reflectivity spectra. The spectra were recorded over the range of 2100A to 4500A and reflectivity peaks were obtained near 2400A and 4100A for GaAs and 2700A and 3700A for Si. The magnitude of these peaks was then observed as a function of annealing parameters. Laser annealing was carried out using a 30 nsec ruby laser pulse. The GaAs samples were implanted 120 KeV Te at a fluence of 10^{14} ions/cm^2; Si samples were implanted —

10 to the 15th power

Sq. cm

with 30 KeV In at a fluence of 10^{15} ions/cm^2. The reflectivity spectrum of implanted GaAs was found to return to that of unimplanted materials at an annealing energy density of approximately 0.35 J/cm^2 whereas the spectrum of Si was found to approach that of the unimplanted samples at energy densities of 1.34 J/cm^2. The values obtained compare well with those obtained from other diagnostic techniques.